Mathematical model of calcium exchange during haemodialysis using a citrate containing dialysate

JULIEN ANIORT

Service de nephrologie, dialyse et tranplantation rénale.
Centre Hospitalier Universitaire Gabriel Montpied, Clermont-Ferrand, France

LAURENT CHUPIN AND NICOLAE CÎNDEA[†]

Université Clermont Auvergne, Laboratoire de Mathématiques Blaise Pascal CNRS-UMR 6620,
Campus des Cézeaux, F-63177 Aubière Cedex, France
[†]Corresponding author. Email: nicolae.cindea@math.univ-bpclermont.fr

Calcium has two important roles in haemodialysis. It participates in the activation of blood coagulation and calcium intakes have a major impact on patient mineral and bone metabolism. The aim of this article is to propose a mathematical model for calcium ions concentration in a dialyzer during haemodialysis using a citrate dialysate. The model is composed of two elements. The first describes the flows of blood and dialysate in a dialyzer fibre. It was obtained by asymptotic analysis and takes into account the anisotropy of the fibres forming a dialyzer. Newtonian and non-Newtonian blood rheologies were tested. The second part of the model predicts the evolution of the concentration of five chemical species present in these fluids. The fluid velocity field drives the convective part of a convection–reaction–diffusion system that models the exchange of free and complexed calcium. We performed several numerical experiments to calculate the free calcium concentration in the blood in a dialyzer using dialysates with or without citrate. The choice of blood rheology had little effect on the fluid velocity field. Our model predicts that only a citrate based dialysate without calcium can decrease free calcium concentration at the blood membrane interface low enough to inhibit blood coagulation. Moreover for a given calcium dialysate concentration, adding citrate to the dialysate decreases total calcium concentration in the blood at the dialyzer outlet. This decrease of the calcium concentration can be compensated by infusing in the dialyzed blood a quantity of calcium computed from the model.

Keywords: haemodialysis; mathematical model; numerical simulations; calcium exchange.

1. Introduction

Renal replacement therapy with haemodialysis is used in patients with end-stage renal disease to remove uremic toxins and restore blood electrolyte composition (Himmelfarb & Ikizler, 2010). End-stage renal disease leads to changes in mineral metabolism, bone disorders and cardiovascular calcifications (Kidney Disease: Improving Global Outcomes (KDIGO)). All are associated with high mortality rates in chronic haemodialysis patients. The balance between calcium intake and loss during haemodialysis treatment affects these abnormalities. It is therefore essential to be able to predict calcium exchange during haemodialysis. Heparin is the most routinely used anticoagulant for the prevention of extracorporeal circulation clotting during haemodialysis sessions. However, heparin exposes the patient to the risk of bleeding complications and heparin-induced thrombocytopenia (Davenport, 2011). To avoid these complications, regional anticoagulation of the blood circuit can be performed with a citrate-containing dialysate (Kossmann *et al.*, 2009). Citrate is a potent calcium chelator that can decrease free calcium

concentration. Calcium ions are required for the activation of coagulation factors. A calcium concentration of less than 0.4 mmol $\cdot$ l^{-1} inhibits blood coagulation (James & Roche, 2004). The anticoagulant properties of citrate dialysate are believed to be caused by a decrease in free calcium concentration of the blood. However, this hypothesis has yet to be confirmed because it is not possible to measure the distribution of free calcium concentration in the dialyzer. In the present study, we use a model of fluid and solute transport to predict calcium concentration in the blood at the outlet of the dialyzer and dialysate and the distribution of free calcium concentration in the dialyzer.

The 1D theory of solute transport in a dialyzer provides a simplified description of solute flows in blood and dialysate channels, assuming that the average concentration of the solute in any cross-section of the channel is equal to the concentration of the solute at the surface of the membrane. Transport in membrane channels was modelled according to the Kedem and Katchalsky equation (Kedem & Katchalsky, 1958) with Villarroel correction (Villarroel *et al.*, 1977) to account for convection–diffusion interaction. One-dimensional axially-dependent models based on ordinary differential equations have provided much insight into the dynamics of fluid and solutes within and around the hollow fibres. However, they have several limitations. Notably, the assumption of homogeneous solute concentration in the cross-section of the channels does not allow the distribution of concentration in the dialyzer to be computed. Resolution of partial differential equations by the finite element method eliminates the need for most of the simplifying assumptions and potentially generates more accurate results.

Few attempts have been made to model calcium flux in a dialyzer. Gotch *et al.* (2007) applied the concept of dialysance to calculate calcium flux through the dialyzer in a similar approach to that used for urea. However, there is no evidence that calcium dialysance is independent of the concentration of calcium and other solutes reacting with calcium. In addition, calcium binding to albumin and diffusible calcium complexes are not taken into account in their calculation (Gotch *et al.*, 2007). Thijssen *et al.* (2010) supplemented the model of Gotch by calculating the concentrations of complexes derived from calcium, citrate and albumin in equilibrium. Only Huang *et al.* (2014) considered the interactions between diffusion, convection and chemical reactions within the dialyzer. Their model is based on one-dimensional theory. They added to their algorithm the calculation of concentrations after the equilibrium of reaction is reached, thereby making it possible to calculate the concentrations within the dialyzer. However, this model, like other 1D models, does not give the concentration gradient of calcium within the blood compartment.

In the present study, we propose a modelling of flows and concentrations, notably those of calcium ions, in a dialyzer using citrate-containing dialysate. The blood is modelled as a Newtonian fluid and as a non-Newtonian fluid. The dialysate fluid is described as a Newtonian fluid and the flow in the membrane is governed by Darcy's equation. The main novel feature of our model with respect to existing flow models (Eloot *et al.*, 2002, 2006; Fasano & Farina, 2012) is in the choice of the boundary conditions that drive the flow. We imposed pressure only at the inlet and outlet of a hollow fibre for the blood and dialysate, respectively. Since these pressures are not generally available at the level of a fibre, we computed the pressure boundary data by an optimization algorithm that provided a set of pressures such that the resulting solution fitted the blood and dialysate global flow rates at the level of the haemodialysis machine. This procedure allow us to study several different rheologies for the non-Newtonian fluid that govern the blood flow and to obtain a velocity field of the fluids in a dialyzer such that the blood flow rate and the dialysate flow rate available on every standard haemodialysis machine are fitted by the model. The velocity field computed by solving the fluid model enters the convective part of the convection–diffusion–reaction system that describes the interaction of five different chemical species related to calcium present in the blood and in dialysate. Since albumin, which is one of the species considered, exerts oncotic pressure in the blood, the model that describes the evolution of the velocity of the fluids should

take into account this supplementary pressure. In this case, the fluid model is strongly coupled to the convection–diffusion–reaction system, which makes the whole system difficult to handle from both theoretical and numerical points of view.

The assumption usually made (Keener & Sneyd, 1998; Legallais *et al.*, 2000) is that oncotic pressure depends non-linearly on the concentration of proteins in the blood. To simplify the model, we assumed that the concentration of proteins in the blood is radially invariant and varies linearly with respect to the longitudinal variable inside a dialyzer's hollow fibre. This assumption is realistic for small ultra-filtration rates, the concentration of proteins in the blood along a hollow fibre having a small variation. The coupled convection, reaction diffusion model, which does not make any assumptions on the concentration of proteins in the blood, will be studied in a future work.

This article is divided into the following sections. In Section 2, we schematically describe the geometry of a dialyzer, which allowed us to introduce the parameters of the model. Section 3 deals with the hydrodynamic flow in a dialyzer's hollow fibre as previously described by Fasano & Farina (2012). Conservation equations are introduced in Section 3.1 to compute fluid velocity and fluid pressure in the blood, the membrane and dialysate. Conditions at the interfaces are provided to couple all the unknowns. After a non-dimensionalization step we simplify the model in Section 3.3, taking into account the low ratio between the width and length of a fibre. Several rheological models for the blood are presented in Section 3.4. The results obtained for different rheologies are compared in Section 3.5 after an explanation of the variational formulation and the numerical scheme used to obtain a solution of the system.

In Section 4, we describe the convection–reaction–diffusion equations used to monitor the concentration of five chemical species present in blood and dialysate fluid. Section 5 illustrates the model introduced in Section 4 by numerical experiments and Section 6 presents a few conclusions and proposes perspectives for this work.

2. Simplified geometry of a dialyzer

The aim of this section is to present the geometrical model considered in this paper in order to propose a mathematical model for the flows of blood and dialysate in a dialyzer fibre.

A dialyzer module consists of an array of a large number N of equispaced parallel hollow fibres. Each fibre is composed of three parts: a central channel, a permeable membrane surrounding this channel and an outer channel delimited by an ideal no-flux boundary confining the permeate flow. The blood flow is confined in the inner channel while the dialysate flows in the outer channel and in the opposite direction. We may focus on studying the flow in a single cell whose geometry is equivalent to the geometry of a pipe with periodic external boundary conditions (see, for instance, Eloot *et al.*, 2002, 2006; Fasano & Farina, 2012 and the references therein). We assume that in each hollow fibre the flows are radially symmetric and, hence, it is natural to work using the cylindrical coordinates. The problem can be reduced to a 2D one in a domain Ω defined by

$$\Omega = \left\{ (x, r) \in \mathbb{R}^2 \mid 0 < x < L \text{ and } 0 < r < R \right\},$$

where L is the length of the fibre and R is its radius. This domain is naturally separated into three sub-domains corresponding to the blood domain Ω_b, the membrane domain Ω_m and the dialysate domain Ω_d, whose dimensions are described by the positive real numbers R_1 and R_2, respectively:

$$\Omega_b = \left\{ (x, r) \in \Omega \mid 0 < r < R_1 \right\},$$

$$\Omega_m = \left\{ (x, r) \in \Omega \mid R_1 < r < R_2 \right\},$$

$$\Omega_d = \left\{ (x, r) \in \Omega \mid R_2 < r < R \right\}.$$

The interfaces between these domains are denoted Γ_{bm} and Γ_{md} and are defined by

$$\Gamma_{bm} = \left\{ (x, r) \in \Omega \mid r = R_1 \right\},$$

$$\Gamma_{md} = \left\{ (x, r) \in \Omega \mid r = R_2 \right\}.$$

Finally, we describe the boundary of the domain as several *natural* sub-boundaries. Therefore, the left side of the rectangle Ω is composed by the union of three segments: $\Gamma_{l,b}$, corresponding to the left side of the blood channel, $\Gamma_{l,m}$, corresponding to the left boundary of the membrane and $\Gamma_{l,d}$ which corresponds to the left side of the dialysate outlet, respectively. The right side of Ω is, symmetrically, formed by three segments $\Gamma_{r,b}$, $\Gamma_{r,m}$ and $\Gamma_{r,d}$. We mention that the blood flows from left to right and the dialysate flows in the opposite direction. All the boundaries are illustrated in Fig. 1 (bottom-right) and precisely described by the following equations:

$$\Gamma_b = \left\{ (x, 0) \in \mathbb{R}^2 \mid x \in (0, L) \right\}, \qquad \Gamma_d = \left\{ (x, R) \in \mathbb{R}^2 \mid x \in (0, L) \right\} \qquad (2.1)$$

$$\Gamma_{bm} = \left\{ (x, R_1) \in \mathbb{R}^2 \mid x \in (0, L) \right\}, \qquad \Gamma_{md} = \left\{ (x, R_2) \in \mathbb{R}^2 \mid x \in (0, L) \right\}, \qquad (2.2)$$

$$\Gamma_{\ell,b} = \left\{ (0, r) \in \mathbb{R}^2 \mid r \in (0, R_1) \right\}, \qquad \Gamma_{r,b} = \left\{ (L, r) \in \mathbb{R}^2 \mid r \in (0, R_1) \right\}, \qquad (2.3)$$

$$\Gamma_{\ell,m} = \left\{ (0, r) \in \mathbb{R}^2 \mid r \in (R_1, R_2) \right\}, \qquad \Gamma_{r,m} = \left\{ (L, r) \in \mathbb{R}^2 \mid r \in (R_1, R_2) \right\}, \qquad (2.4)$$

$$\Gamma_{\ell,d} = \left\{ (0, r) \in \mathbb{R}^2 \mid r \in (R_2, R) \right\}, \qquad \Gamma_{r,d} = \left\{ (L, r) \in \mathbb{R}^2 \mid r \in (R_2, R) \right\}. \qquad (2.5)$$

Due to the large difference between the two lengths L and R (typically $L = 23$ cm and $R = 0.23$ mm), it will be interesting to work in a re-scaled domain. This anisotropy is discussed in Section 3. Finally, the schematic simplification of the geometry of the dialyzer is described in Fig. 1.

3. Modelling of flow in a fibre

This section proposes a model for the fluid flow inside a hollow fibre in a dialyzer.

3.1 *Governing equations*

The flow in a fibre is characterized by its velocity field and its pressure. The model described here is based on the physical conservation of mass and momentum, and it is first introduced on each sub-domain corresponding to the blood domain, to the membrane and to the dialysate domain, respectively. The notations and the physical model for each sub-domain are given in Table 1. Some interface conditions are next introduced between these connected domains.

3.1.1 *Blood flow* The blood is modelled either as a Newtonian fluid, either as a quasi-Newtonian fluid. The equations satisfied by the velocity field (v_x, v_r) and the pressure p_b correspond to the mass and the
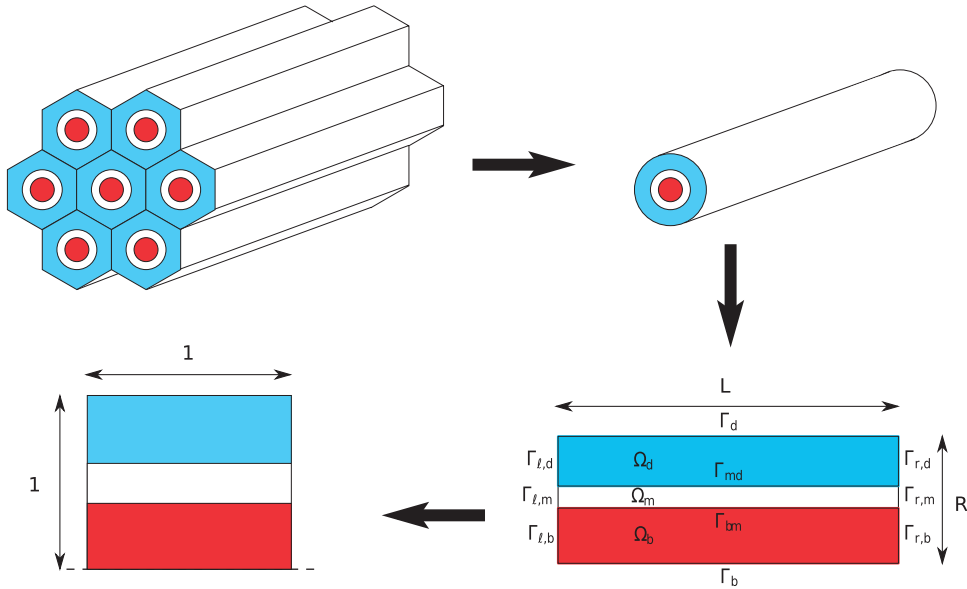
FIG. 1. The reduction process of the initial problem in a complex physical geometry to a problem in a square: firstly, considering only one fibre; secondly, using cylindrical coordinates; thirdly, scaling the domain.

TABLE 1 *Notation for pressure, velocity fields and the physical model corresponding to the three sub-domains of domain Ω*

Domain	Pressure	Velocity	Model
Blood: Ω_b	p_b	(v_x, v_r)	Non-Newtonian fluid
Membrane: Ω_m	p_m	(u_x, u_r)	Darcy's equation
Dialysate: Ω_d	p_d	(w_x, w_r)	Newtonian fluid

momentum conservation laws. These equations are valid for $(x, r) \in \Omega_b$ and for any time $t > 0$:

$$
\begin{cases}
\rho\left(\partial_t v_x + v_x \partial_x v_x + \frac{1}{r} v_r \partial_r (r v_x)\right) = -\partial_x p_b + 2\mu\, \partial_x\left(G(\dot{\gamma})\, \partial_x v_x\right) + \frac{\mu}{r}\partial_r\left(r\, G(\dot{\gamma})\, (\partial_r v_x + \partial_x v_r)\right), \\
\rho\left(\partial_t v_r + v_x \partial_x v_r + \frac{1}{r} v_r \partial_r (r v_r)\right) = -\partial_r p_b + 2\frac{\mu}{r}\partial_r\left(r\, G(\dot{\gamma})\, \partial_r v_r\right) + \mu\, \partial_x\left(G(\dot{\gamma})\, (\partial_r v_x + \partial_x v_r)\right), \\
\partial_x v_x + \frac{1}{r}\partial_r (r v_r) = 0.
\end{cases}
$$

The constant blood density is denoted by $\rho = 10^3 \,\text{kg} \cdot \text{m}^{-3}$. We consider several different rheology models for the blood. The viscosity of the blood is given by $\mu\, G(\dot{\gamma})$, where G is a function depending on

the shear rate:

$$\dot{\gamma} = \sqrt{|\partial_x v_x|^2 + |\partial_r v_r|^2 + \left|\frac{v_r}{r}\right|^2 + \frac{1}{2}|\partial_r v_x + \partial_x v_r|^2}.$$

Here and henceforth, μ denotes the reference viscosity and is equal to the viscosity of the water ($\mu = 10^{-3}$ Pa $\cdot$ s). Some examples of functions G are given in Section 3.4.

3.1.2 *Membrane flow* In the porous membrane, the governing equations are the continuity equation (corresponding to the free-divergence of the flux) coupled with Darcy's law (corresponding to the fact that the flux is proportional to the gradient of the pressure p_m). For $(x, r) \in \Omega_m$, these two equations give:

$$\partial_x^2 p_m + \frac{1}{r}\partial_r(r\partial_r p_m) = 0.$$

The velocity field in the membrane is denoted by (u_x, u_r) and is obtained from the following relations

$$\begin{cases} u_x = -\dfrac{K}{\mu}\partial_x p_m, \\ u_r = -\dfrac{K}{\mu}\partial_r p_m, \end{cases}$$

the coefficient K corresponding to the permeability of the membrane.

3.1.3 *Dialysate flow* The dialysate is supposed to be a Newtonian fluid with the same constant density as the blood, and with a viscosity equal to the reference viscosity μ. Navier–Stokes equations on the velocity (w_x, w_r) and the pressure p_d read, for $(x, r) \in \Omega_d$ and for any time $t > 0$:

$$\begin{cases} \rho\left(\partial_t w_x + w_x\partial_x w_x + \dfrac{1}{r}w_r\partial_r(rw_x)\right) = -\partial_x p_d + \mu\partial_x^2 w_x + \dfrac{\mu}{r}\partial_r(r\partial_r w_x), \\ \rho\left(\partial_t w_r + w_x\partial_x w_r + \dfrac{1}{r}w_r\partial_r(rw_r)\right) = -\partial_r p_d + \dfrac{\mu}{r}\partial_r(r\partial_r w_r) + \mu\partial_x^2 w_r, \\ \partial_x w_x + \dfrac{1}{r}\partial_r(rw_r) = 0. \end{cases}$$

3.1.4 *Interface blood-membrane* The conditions imposed at the interface blood/membrane Γ_{bm} correspond to the continuity of the flux, Saffman's condition for the slip velocity (see for instance Fasano & Farina, 2012), and the continuity of the pressure, respectively. For every $(x, r) \in \Gamma_{bm}$, these conditions write as follows:

$$\begin{cases} v_r = -\dfrac{K}{\mu}\partial_r p_m, \\ -\partial_r v_x = \dfrac{\alpha_{\text{BJ}}}{\sqrt{K}}v_x, \\ p_m = p_b - p_o, \end{cases}$$

where the coefficient α_{BJ} is the Beavers–Joseph constant (measured slip coefficient only depends on porous media properties) relative to the porous wall.

The oncotic pressure p_o depends on the concentration of the suspended proteins in the blood. In what follows, we assume that the oncotic pressure is constant with respect to the radial variable r and depends non-linearly on the spatial variable x. More precisely, following Legallais *et al.* (2000, Equation (20)), the oncotic pressure is given by

$$p_o(x) = 2.1 \times 10^{-1} c_p(x) + 1.6 \times 10^{-3} c_p(x)^2 + 9 \times 10^{-6} c_p(x)^3, \tag{3.1}$$

where $c_p(x)$ is the concentration of proteins at $(x, r) \in \Omega_b$. Nevertheless, since the spatial distribution of proteins in the blood inside a dialyzer fibre is *a priori* unknown, we assume that this concentration varies linearly with respect to the longitudinal variable x.

3.1.5 *Interface membrane-dialysate*   The conditions on the interface membrane/dialysate Γ_{md} are similar to the conditions on the interface blood/membrane, with the difference that the Beavers–Joseph constant appearing here is different to the one appearing for Γ_{bm} and there is no oncotic pressure acting on this interface. More precisely, for every $(x, r) \in \Gamma_{md}$ we have:

$$\begin{cases} w_r = -\dfrac{K}{\mu} \partial_r p_m, \\[2mm] \partial_r w_x = \dfrac{\beta_{BJ}}{\sqrt{K}} w_x, \\[2mm] p_m = p_d, \end{cases}$$

where the coefficient β_{BJ} is another Beavers–Joseph constant relative to the porous membrane.

3.1.6 *Boundary conditions for the flow*   The boundary of the domain is composed of the lateral boundaries described by $x = 0$ and $x = L$, by the 'exterior' boundary $r = R$ and by the symmetry axis $r = 0$. The physical conditions on these boundaries are given by:

$p_b = p_{b,\text{in}}$ on $\Gamma_{\ell,b}$,	$p_b = p_{b,\text{out}}$ on $\Gamma_{r,b}$		for the blood pressure;
$p_d = p_{d,\text{in}}$ on $\Gamma_{r,d}$,	$p_d = p_{d,\text{out}}$ on $\Gamma_{\ell,d}$		for the dialysate pressure;
$w_r = 0$ on Γ_d,	$\partial_r w_x = 0$ on Γ_d,	$\partial_r p_d = 0$ on Γ_d	top boundary;
$\partial_r v_x = 0$ on Γ_b	$v_r = 0$ on Γ_b,	$\partial_r p_b = 0$ on Γ_b	symmetry axis.

The first boundary conditions correspond to the imposed pressures on the blood and on the dialysate. An assumption usually made in the literature is that these pressures satisfy $p_{b,\text{in}} > p_{b,\text{out}} > p_{d,\text{in}} > p_{d,\text{out}}$ (see Eloot *et al.*, 2002, 2006 or Fasano & Farina, 2012, Table 3 for typical values of these pressures). The conditions on the top boundary Γ_d correspond to the radial periodicity of the dialyzer's structure described in Fig. 1 and the conditions on Γ_b to the radial symmetry of the domain.

In order to have a well posed system, we complete these boundary conditions by considering homogeneous Neumann boundary conditions on the other parts of the boundary of Ω:

$$\partial_x v_x = \partial_x v_r = 0 \qquad \text{on } \Gamma_{\ell,b} \cup \Gamma_{r,b},$$

$$\partial_x w_x = \partial_x w_r = 0 \qquad \text{on } \Gamma_{\ell,d} \cup \Gamma_{r,d},$$

$$\partial_x p_m = 0 \qquad \text{on } \Gamma_{\ell,m} \cup \Gamma_{r,m}.$$

These conditions, acting on the lateral boundaries, impose the fact that the velocity and the pressure are locally constant in the longitudinal direction at both extremities of the fibre. All these homogeneous Neumann boundary conditions appear naturally in the variational formulation described in Appendix B.

3.2 *Scaling procedure*

In this section, we replace the physical quantities appearing in the model by their corresponding dimensionless quantities, and we rewrite in consequence the equations. First, we set the reference density ρ and the reference viscosity μ to the density and the viscosity of water:

$$\rho = 10^3 \, \text{kg} \cdot \text{m}^{-3}, \qquad \mu = 10^{-3} \, \text{Pa} \cdot \text{s}.$$

In Table 2, we gather two sets of parameters describing the geometry and the permeability of two typical dialyzers. The first set of parameters describe the dialyzer machine in Eloot *et al.* (2002) and the second one lists the product specifications of a universal dialyzer APS-18U ®. Typical values for blood injection/output pressures ($p_{b,\text{in}}$ and $p_{b,\text{out}}$) and dialysate injection/output pressures ($p_{d,\text{in}}$ and $p_{d,\text{out}}$) are given in (3.2) (see also Eloot *et al.*, 2002; Fasano & Farina, 2012):

$$p_{b,\text{in}} = 16 \times 10^3 \, \text{Pa}, \quad p_{b,\text{out}} = 11 \times 10^3 \, \text{Pa}, \quad p_{d,\text{in}} = 10^3 \, \text{Pa}, \quad p_{d,\text{out}} = 0.1 \times 10^3 \, \text{Pa}. \tag{3.2}$$

3.2.1 *Reference quantities*   Some characteristic sizes appear naturally in the formulation of the problem: two lengths L and R, and four pressures: $p_{b,\text{in}}, p_{b,\text{out}}, p_{d,\text{in}}$ and $p_{d,\text{out}}$. In practice, we use the difference

$$P = p_{b,\text{in}} - p_{b,\text{out}}$$

as a reference pressure. Using this reference pressure, the reference viscosity μ and the two characteristic lengths R and L, it is possible to define a reference velocity:

$$V = \frac{PR^2}{\mu L}.$$

It is also possible to introduce another reference pressure using the difference $p_{d,\text{in}} - p_{d,\text{out}}$. The corresponding velocity, denoted W, is given by $W = \mathscr{P}_1 V$ where

$$\mathscr{P}_1 = \frac{p_{d,\text{in}} - p_{d,\text{out}}}{P}. \tag{3.3}$$

TABLE 2 *Two set of values describing two different dialyzers*

Name	Notation	Set A		Set B	
Length	L	2.3×10^{-1}	m	3.3×10^{-1}	m
Total radius	R	2.3×10^{-4}	m	2.1×10^{-4}	m
Blood radius	R_1	10^{-4}	m	10^{-4}	m
Membrane radius	R_2	1.4×10^{-4}	m	1.45×10^{-4}	m
Permeability	K	2.4×10^{-18}	m²	1.21×10^{-17}	m²
Number of fibres	N	10^4		10^4	

In order to take into account all the pressures imposed on the boundaries of the domain, we define a new dimensionless number

$$\mathscr{P}_2 = \frac{p_{b,\text{out}} - p_{d,\text{in}}}{P}. \tag{3.4}$$

We note that the first velocity V is used for the non-dimensionalization of the blood velocity whereas the second velocity W is employed to non-dimensionalize the dialysate velocity. Finally, we introduce the reference time

$$T = \frac{L}{V}.$$

3.2.2 *Dimensionless numbers*   The following dimensionless numbers can be defined:

$$\varepsilon = \frac{R}{L}, \quad \mathscr{R}e = \frac{\rho R V}{\mu}, \quad \mathscr{D}a = \frac{K}{R^2}, \quad B_b = \frac{\alpha_{\text{BJ}}}{\sqrt{\mathscr{D}a}}, \quad B_d = \frac{\beta_{\text{BJ}}}{\sqrt{\mathscr{D}a}}.$$

These numbers are used to write the complete system of partial differential equations in a dimensionless form. The first parameter describes the ratio between the two lengths previously introduced. In practice, the number ε is much smaller than 1 and the Reynolds number $\mathscr{R}e$ will be of order 1. The number $\mathscr{D}a$ corresponds to the Darcy number and the quotient $\mathscr{D}a/\varepsilon^2$ is of order 1. It is more difficult to evaluate the Beaver-Joseph coefficients α_{BJ} and β_{BJ}. These parameters depend on the properties of the porous material as well as the material's specific surface conditions. In Neale & Nader (1974) and more recently in Beck *et al.* (2014), the authors take $\beta_{\text{BJ}} = 1$. We adopt this hypothesis for the present work. In this case, the product εB_d is of order 1, and this corresponds to the Remark 3 in (Fasano & Farina, 2012, page 1918). Following Fasano & Farina (2012) again, the boundary condition on the interface blood-membrane must come into play. They propose to use a coefficient α_{BJ} such that the parameter B_b is of order 1 with respect to ε, and we use the value given as example in Fasano & Farina (2012, Table 7). This difference between the two Beavers–Joseph's coefficients is related to the fact that, contrary to the dialysate, the blood does not adhere at the membrane surface.

We list below an example of non-dimensional numbers corresponding to Set A of data in Table 2 (see Fasano & Farina, 2012, Remark 3 for the typical values of Beavers–Joseph number B_d which is assumed to be large, typically of order of $1/\varepsilon$):

$$\varepsilon = 10^{-3}, \quad \mathscr{R}e = 124.836, \quad \mathscr{D}a = 4.537 \times 10^{-11}, \quad B_b = 2.5, \quad B_d = 7.3 \times 10^3.$$

We use the following scaling for the different variables (the star notation $\star$ corresponding to variables without dimension):

$$x = L x^\star, \quad r = R r^\star, \quad t = T t^\star, \quad p_a = p_{b,\text{out}} + P p_a^\star, \quad \text{for } a \in \{b, m, d, o\},$$

$$v_x = V v_x^\star, \quad v_r = \varepsilon V v_r^\star, \quad u_x = W u_x^\star, \quad u_r = \varepsilon W u_r^\star \quad w_x = W w_x^\star, \quad w_r = \varepsilon W w_r^\star.$$

Note that, since the pressure is defined up to an additive constant, we choose $p_{b,\text{out}}$ as a reference pressure. It is then possible to rewrite all the equations describing the flow under a dimensionless form. For clarity, these equations are postponed in the Appendix A. We only indicate here the domains in which the equations hold since this notation will be reused in the following sections.

Firstly, the domain Ω becomes, after the scaling, the unit square ω:

$$\omega = \left\{ (x^\star, r^\star) \in \mathbb{R}^2 \quad ; \quad 0 < x^\star < 1 \quad \text{and} \quad 0 < r^\star < 1 \right\}.$$

Similarly to domain Ω, the rescaled domain ω is composed of three subdomains:

$$\omega_b = \left\{ (x^\star, r^\star) \in \omega \quad ; \quad 0 < r^\star < \frac{R_1}{R} \right\},$$

$$\omega_m = \left\{ (x^\star, r^\star) \in \omega \quad ; \quad \frac{R_1}{R} < r^\star < \frac{R_2}{R} \right\},$$

$$\omega_d = \left\{ (x^\star, r^\star) \in \omega \quad ; \quad \frac{R_2}{R} < r^\star < 1 \right\},$$

and its boundary is formed by the following segments:

$$\gamma_b = \left\{ (x^\star, 0) \in \mathbb{R}^2 \quad ; \quad x^\star \in (0,1) \right\}, \qquad \gamma_d = \left\{ (x^\star, 1) \in \mathbb{R}^2 \quad ; \quad x^\star \in (0,1) \right\},$$

$$\gamma_{bm} = \left\{ \left(x^\star, \frac{R_1}{R} \right) \in \mathbb{R}^2 \quad ; \quad x^\star \in (0,1) \right\}, \qquad \gamma_{md} = \left\{ \left(x^\star, \frac{R_2}{R} \right) \in \mathbb{R}^2 \quad ; \quad x^\star \in (0,1) \right\},$$

$$\gamma_{\ell,b} = \left\{ (0, r^\star) \in \mathbb{R}^2 \quad ; \quad r^\star \in \left(0, \frac{R_1}{R} \right) \right\}, \qquad \gamma_{r,b} = \left\{ (1, r^\star) \in \mathbb{R}^2 \quad ; \quad r^\star \in \left(0, \frac{R_1}{R} \right) \right\},$$

$$\gamma_{\ell,m} = \left\{ (0, r^\star) \in \mathbb{R}^2 \quad ; \quad r^\star \in \left(\frac{R_1}{R}, \frac{R_2}{R} \right) \right\}, \qquad \gamma_{r,m} = \left\{ (1, r^\star) \in \mathbb{R}^2 \quad ; \quad r^\star \in \left(\frac{R_1}{R}, \frac{R_2}{R} \right) \right\},$$

$$\gamma_{\ell,d} = \left\{ (0, r^\star) \in \mathbb{R}^2 \quad ; \quad r^\star \in \left(\frac{R_2}{R}, 1 \right) \right\}, \qquad \gamma_{r,d} = \left\{ (1, r^\star) \in \mathbb{R}^2 \quad ; \quad r^\star \in \left(\frac{R_2}{R}, 1 \right) \right\}.$$

3.3 *Considerations on the geometric anisotropy of a fibre*

During the scaling process, we introduced a dimensionless number ε which is very small with respect to 1. To obtain a simpler system, we will keep only the main order terms with respect to ε, taking into account that

$$\widetilde{\mathscr{D}a} = \frac{\mathscr{D}a}{\varepsilon^2} = \mathscr{O}(1) \quad \text{and} \quad B_d = \mathscr{O}\!\left(\frac{1}{\varepsilon} \right),$$

all the other parameters being of order 1. Considering this anisotropy ($\varepsilon \ll 1$), we can formally simplify the set of equations describing the flow. More precisely, the equations obtained in Appendix A can be approximated by the equations described below.

For every $(x^\star, r^\star) \in \omega_b$ the simplified blood flow is governed by the following system

$$
\begin{cases}
0 = -\partial_{x^\star} p_b^\star + \dfrac{1}{r^\star} \partial_{r^\star} \left(r^\star \widetilde{G}(\dot{\gamma}) \, \partial_{r^\star} v_x^\star \right) - \partial_{x^\star} p_o^\star, & \text{(3.5a)} \\[2mm]
0 = -\partial_{r^\star} p_b^\star, & \text{(3.5b)} \\[2mm]
\partial_{x^\star} v_x^\star + \dfrac{1}{r^\star} \partial_{r^\star} (r^\star v_r^\star) = 0, & \text{(3.5c)}
\end{cases}
$$

where the shear rate reduces to $\dot{\gamma} = \dfrac{1}{\varepsilon\sqrt{2}} |\partial_{r^\star} v_x^\star|$, and the function $\widetilde{G}$ is defined from the viscosity function G as follows

$$
\widetilde{G}(X) = G\left(\frac{\varepsilon^2 P}{\mu} X \right). \tag{3.6}
$$

The pressure and the velocities into the membrane domain ω_m satisfy

$$
\begin{cases}
\partial_{r^\star} (r^\star \partial_{r^\star} p_m^\star) = 0, & \text{(3.7a)} \\[2mm]
u_x^\star = 0, & \text{(3.7b)} \\[2mm]
u_r^\star = -\dfrac{\widetilde{\mathscr{D}} a}{\mathscr{P}_1} \partial_{r^\star} p_m^\star, & \text{(3.7c)}
\end{cases}
$$

and the dialysate flow is given by the solution of the following equation:

$$
\begin{cases}
0 = -\partial_{x^\star} p_d^\star + \dfrac{\mathscr{P}_1}{r^\star} \partial_{r^\star} (r^\star \partial_{r^\star} w_x^\star), & \text{(3.8a)} \\[2mm]
0 = -\partial_{r^\star} p_d^\star, & \text{(3.8b)} \\[2mm]
\partial_{x^\star} w_x^\star + \dfrac{1}{r^\star} \partial_{r^\star} (r^\star w_r^\star) = 0. & \text{(3.8c)}
\end{cases}
$$

Finally, the simplified conditions at the interfaces blood/membrane, membrane/dialysate and at the exterior boundaries become:

- interface blood/membrane (on γ_{bm}):

$$
\begin{cases}
v_r^\star = -\widetilde{\mathscr{D}} a \, \partial_{r^\star} p_m^\star, & \text{(3.9a)} \\[2mm]
-\partial_{r^\star} v_x^\star = B_b v_x^\star, & \text{(3.9b)} \\[2mm]
p_m^\star = p_b^\star - p_o^\star. & \text{(3.9c)}
\end{cases}
$$

- interface membrane/dialysate (on γ_{md}):

$$\begin{cases} w_r^{\star} = -\dfrac{\widetilde{\mathscr{D}}a}{\mathscr{P}_1}\partial_{r^{\star}}p_m^{\star}, & \text{(3.10a)} \\[2mm] w_x^{\star} = 0, & \text{(3.10b)} \\[2mm] p_m^{\star} = p_d^{\star}. & \text{(3.10c)} \end{cases}$$

- exterior boundary conditions:

$$\begin{cases} p_b^{\star}|_{\gamma_{\ell,b}} = 1, & p_b^{\star}|_{\gamma_{r,b}} = 0, & \text{(3.11a)} \\[2mm] p_d^{\star}|_{\gamma_{r,d}} = -\mathscr{P}_2, & p_d^{\star}|_{\gamma_{\ell,d}} = -\mathscr{P}_2 - \mathscr{P}_1, & \text{(3.11b)} \\[2mm] w_r^{\star}|_{\gamma_d} = \partial_{r^{\star}}w_x^{\star}|_{\gamma_d} = 0, & & \text{(3.11c)} \\[2mm] \partial_{r^{\star}}v_x^{\star}|_{\gamma_b} = 0. & & \text{(3.11d)} \end{cases}$$

REMARK 3.1   It is not difficult to determine the membrane pressure $p_m^{\star}$. This pressure satisfies the ordinary differential equation (3.7a) within the two boundary Dirichlet conditions (3.9c) and (3.10c). We deduce the following expression of $p_m^{\star}$ with respect to the pressures $p_b^{\star}$ and $p_d^{\star}$: for $(x^{\star}, r^{\star}) \in \omega_m$,

$$p_m^{\star}(x^{\star}, r^{\star}) = \frac{1}{\ln(R_2/R_1)}\Big((p_d^{\star}(x^{\star}) - p_b^{\star}(x^{\star}) + p_o^{\star}(x^{\star}))\ln(Rr^{\star}) + (p_b^{\star}(x^{\star}) - p_o^{\star}(x^{\star}))\ln R_2 - p_d^{\star}(x^{\star})\ln R_1 \Big).$$

Moreover, the derivative of $p_m^{\star}$ with respect to $r^{\star}$ (appearing in the other equations) reads

$$\partial_{r^{\star}}p_m^{\star}(x^{\star}, r^{\star}) = \frac{p_d^{\star}(x^{\star}) - p_b^{\star}(x^{\star})p_o^{\star}(x^{\star})}{r^{\star}\ln(R_2/R_1)}.$$

In particular, we can express the fluid velocity in the membrane as:

$$u_x^{\star}(x^{\star}, r^{\star}) = 0 \quad \text{and} \quad u_r^{\star}(x^{\star}, r^{\star}) = -\frac{\widetilde{\mathscr{D}}a}{\mathscr{P}_1}\frac{p_d^{\star}(x^{\star}) - p_b^{\star}(x^{\star}) + p_o^{\star}(x^{\star})}{r^{\star}\ln(R_2/R_1)}.$$

REMARK 3.2   When the blood is considered as a Newtonian fluid, an analytical expression of the simplified system (3.5a)–(3.11d) can be obtained (see Fasano & Farina, 2012 for details).

REMARK 3.3   By ignoring the terms of order ε, the simplified system will not depend on the time any more. In other words, among other simplifications, we are searching for a stationary solution of the system considered in Appendix A.

3.4 *Different rheological models for blood*

As indicated above, the blood is generally considered as a Newtonian fluid, or as a quasi-Newtonian fluid. Its viscosity is assumed to be variable and is described by a function G, or, equivalently, by its corresponding dimensionless version $\widetilde{G}$. More precisely, we recall that we have the following relation between the viscosity and the function G:

$$\text{Viscosity} = \mu\,G(\dot{\gamma}),$$

TABLE 3 *Non-Newtonian blood viscosity models*

Model	Description
Power-law model	$\widetilde{G}(X) = m \left(\dfrac{\varepsilon^2 P}{\mu} \right)^{n-1} X^{n-1}$
	$m = 4.25$
	$n = 0.7755$
Carreau model	$\widetilde{G}(X) = \dfrac{1}{\mu} \left(\mu_\infty + \left(\mu_0 - \mu_\infty \right) \left(1 + (\lambda^\star X)^2 \right)^{\frac{n-1}{2}} \right)$
	$\mu_0 = 0.056 \,\mathrm{Pa \cdot s}$
	$\lambda^\star = \dfrac{\varepsilon^2 P}{\mu} \lambda, \;\text{with } \lambda = 3.131\,\mathrm{s}$
	$n = 0.3568$
Quemada model	$\widetilde{G}(X) = \dfrac{\mu_p}{\mu} \left(1 - \dfrac{1}{2} \dfrac{k_0 + k_\infty \sqrt{X/\gamma^\star}}{1 + \sqrt{X/\gamma^\star}} \phi \right)^{-2}$
	$\mu_p = 1.2 \times 10^{-3}\,\mathrm{Pa \cdot s}$
	$\phi = 0.4$
	$k_0 = 4.65, \; k_\infty = 1.84$
	$\gamma^\star = \gamma_c \dfrac{\mu}{\varepsilon^2 P}, \;\text{with } \gamma_c = 2.23\,\mathrm{s^{-1}}$
Cross model	$\widetilde{G}(X) = \dfrac{1}{\mu} \left(\mu_\infty + (\mu_0 - \mu_\infty) \left(1 + \left(\dfrac{X}{\gamma^\star} \right)^n \right)^{-1} \right)$
	$\mu_0 = 0.0364$
	$\gamma^\star = \gamma_c \dfrac{\mu}{\varepsilon^2 P}, \;\text{with } \gamma_c = 2.63\,\mathrm{s^{-1}}$
	$n = 1.45$

where μ is the reference viscosity and $\dot{\gamma}$ corresponds to the shear rate. In particular, when the blood is modelled as a Newtonian fluid, its viscosity is constant and is given by

$$\mu_\infty = 3.45 \times 10^{-3}\,\mathrm{Pa \cdot s}. \tag{3.12}$$

Recalling from Table 2 that the reference viscosity is $\mu = 10^{-3}\,\mathrm{Pa \cdot s}$, it follows that $\widetilde{G}(X) = 3.45$ for this Newtonian model.

In Table 3, we summarize different widely used non-Newtonian constitutive relationships for the blood viscosity model against the shear rate. For more details concerning these non-Newtonian blood viscosity models we refer the reader to Mamun Molla & Paul (2012).

In order to compare the rheology models mentioned in this section, we numerical computed the minimal and the maximal values of the shear rate $\dot{\gamma}$ appearing along the iterations in the fixed point algorithm used to tackle the non-linearity given by $\widetilde{G}$. We obtained that the values $\dot{\gamma}$ are mainly distributed in the interval $[10^{-4}, 10^2]$. Plotting the function $\widetilde{G}(X)$ on this interval, we easily observe that all the considered models, at the exception of the power-law model, are similar to the Newtonian one for values of X close to 10^2, having slightly different behaviours when X goes to zero.

3.5 *Numerical simulations of the flows within a fibre*

To numerically approach a solution of the previous systems, we first consider their weak formulations. For the interested reader, these weak formulations are given Appendix B. In order to solve the weak formulations we use the finite element method combined with a fixed point strategy employed for taking into account the non-linearity given by $\widetilde{G}$. We use $\mathbb{P}_1$-bubble finite elements to represent the velocities ($w_x^\star$, $w_r^\star$, $v_x^\star$ and $v_r^\star$) and $\mathbb{P}_1$ finite elements for the pressures ($p_b^\star$ and $p_d^\star$). For the numerical implementation, `FreeFem++` Hecht (2012) is employed.

3.5.1 *Effective computations of the flows—the case of pressure data*   In the simplest case we assume that all the data in Tables 2 and the pressures (3.2) are known, as well as the non-linearity $\widetilde{G}$. For the results in this Section, the geometry of the dialyzer is the one described by Set A in Table 2. We then compute the non-dimensional numbers, $\mathscr{D}a$, B_b, $\mathscr{P}_1$ and $\mathscr{P}_2$ in order to numerically approach the solution of the variational formulations given in Appendix B.

The velocity in the entire domain ω is denoted $(U_x^\star, U_r^\star)$ and is linked to the velocities in the blood, in the membrane and in the dialysate as follows:

$$
(U_x^\star, U_r^\star) = \begin{cases} (v_x^\star, v_r^\star) & \text{in } \omega_b, \\ (u_x^\star, u_r^\star) & \text{in } \omega_m, \\ (w_x^\star, w_r^\star) & \text{in } \omega_d. \end{cases}
$$

We denote (U_x, U_r) the physical velocity which is thus defined on the physical domain Ω.

Using the boundary values for pressures p_b and p_d prescribed in (3.2), the influence of the rheologies proposed in Section 3.4 on the velocity field is illustrated in Fig. 2. We remark that the choice of the rheology governing the blood flow has an influence on the horizontal velocity profile in the domain Ω_b and almost no influence on the radial blood flow or on both flows in domains Ω_m and Ω_d.

As an example, we choose to illustrate only the Newtonian model and the power-law model for the rheology of the blood. The pressure and the velocity in domains Ω_b, Ω_m and Ω_d, obtained again for the boundary values for the pressure given by (3.2), are displayed in Figs 3 and 4, respectively. We remark that the pressure profiles are very similar for both models and, as expected, the dependence of the velocity on the rheology of the blood is most important in Ω_b.

We mention that we obtained very similar flow rates for the blood and the dialysate as the ones previously obtained in Eloot *et al.* (2002) for the same choice of pressure data, the same geometry and a similar blood rheology.

3.5.2 *Effective computations of the flows − the case of flow rates data*   We consider now a case which, on one hand, is more complex from the numerical point of view, and on the other hand, more natural from an experimental point of view, the pressures on boundaries $\Gamma_{\ell,b}$, $\Gamma_{r,b}$ and $\Gamma_{\ell,d}$, $\Gamma_{r,d}$
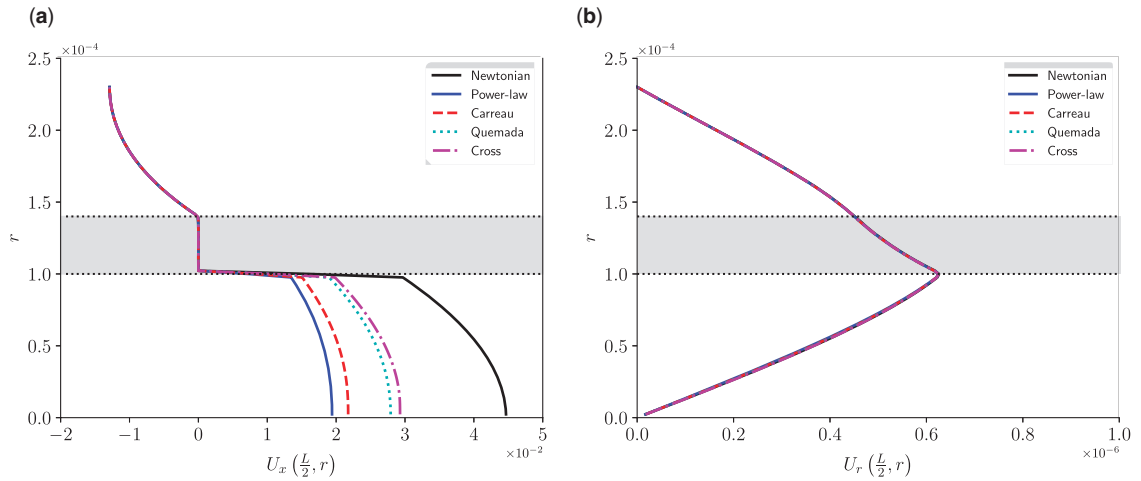
FIG. 2. Velocity profiles on the line $x = \dfrac{L}{2}$ corresponding to the geometry parameters in Table 2 (Set A) and the pressure boundary data (3.2). (a) Values (in m · s^{-1}) of the longitudinal component of the velocity $U_x(\frac{L}{2}, r)$ for $r \in (0, R)$. (b) Values (in m · s^{-1}) of the radial component of the velocity $U_r(\frac{L}{2}, r)$ for $r \in (0, R)$.
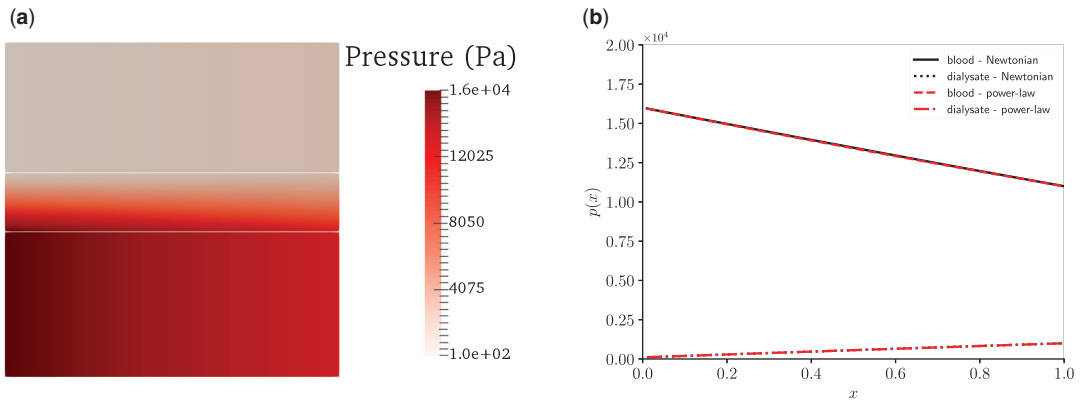

FIG. 3. Pressure (in Pa) corresponding to the power-law model, the geometric parameters in Table 2 and the boundary values given by (3.2). (a) Spatial distribution in domain Ω. (b) Longitudinal profile of pressure in blood and dialysate.

$(\vec{P} = (p_{b,\text{in}}, p_{b,\text{out}}, p_{d,\text{in}}, p_{d,\text{out}}))$ are not available, and we only dispose of the fluxes $\vec{Q}$ at the entrance and at the exit of dialyzer. Since the number of fibres composing the dialyzer and their geometry are known, we can easily deduce from the fluxes $\vec{Q} = (Q_{b,\text{in}}, Q_{b,\text{out}}, Q_{d,\text{in}}, Q_{d,\text{out}})$ the fluxes at the entrance and exit of domains Ω_b and Ω_d. An example of such fluxes is given in Table 4. These flow rates are directly determined given the velocity field. For instance, the blood flux at the entrance of the domain Ω_b is related to the blood injection flux by the following relation:

$$Q_{b,\text{in}} = 2\pi N \int_0^{R_1} v_x(0, r)\, r\, \mathrm{d}r,$$
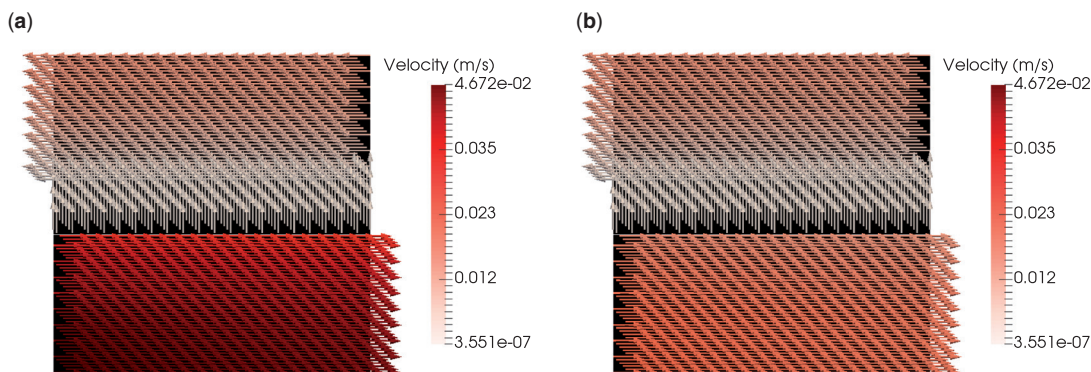
(a)

(b)

FIG. 4. Velocity magnitude of fluids in Ω corresponding to Newtonian model (a) and power-law model (b) geometric parameters in Table 2 Set A and pressure boundary data 3.2.

TABLE 4 *Typical values for the fluxes for clinical dialysis*

Name	Notation	EX1 (ml·min^{-1})	EX2 (ml·min^{-1})
Blood injection flux	$Q_{b,\text{in}}$	300	400
Blood output flux	$Q_{b,\text{out}}$	290	390
Dialysate injection flux	$Q_{d,\text{in}}$	500	500
Dialysate output flux	$Q_{d,\text{out}}$	510	510

where N is the number of hollow fibres composing the dialyzer. It is therefore relatively easy to determine the fluxes $\vec{Q}$ from the pressures $\vec{P}$ using the procedure proposed above; we denote by Φ the application associating to a given pressure vector $\vec{P}$ the corresponding fluxes vector $\vec{Q}$. The reverse is much less obvious. We propose an optimization algorithm to determine a set of pressures from the fluxes. Given the flow rates $\vec{Q}$, we will minimize the following function:

$$\mathscr{J}(\vec{P}) = \frac{1}{2}\|\Phi(\vec{P}) - \vec{Q}\|^2, \tag{3.13}$$

where $\|\cdot\|$ is the usual euclidean norm on $\mathbb{R}^4$. To this purpose, we implemented a gradient-type algorithm described in Appendix 1 (in practice, this algorithm is used with the following numerical parameters: $h = \varepsilon_1 = 1$, and $\alpha_0 = 10^3$). Remark that the pressure data minimizing $\mathscr{J}$ may not be unique.

   With the flux data instead of the pressure data (i.e. using Table 4 instead of the values in (3.2)), we compute the velocity of the fluids for the rheological models proposed in Section 3.4. The vertical and horizontal velocity profiles obtained for different blood rheologies and for pressures data (EX1) are illustrated in Fig. 5. The results in this subsection correspond to a dialyzer described by Set B in Table 2.

REMARK 3.4 Unlike the results illustrated in Fig. 2(a), we observe that the longitudinal velocities displayed in Fig. 5(a) present much less variation with respect to the choice of the model. This is a consequence of the fact that for the simulations in Fig. 5, for each one of the rheologies considered
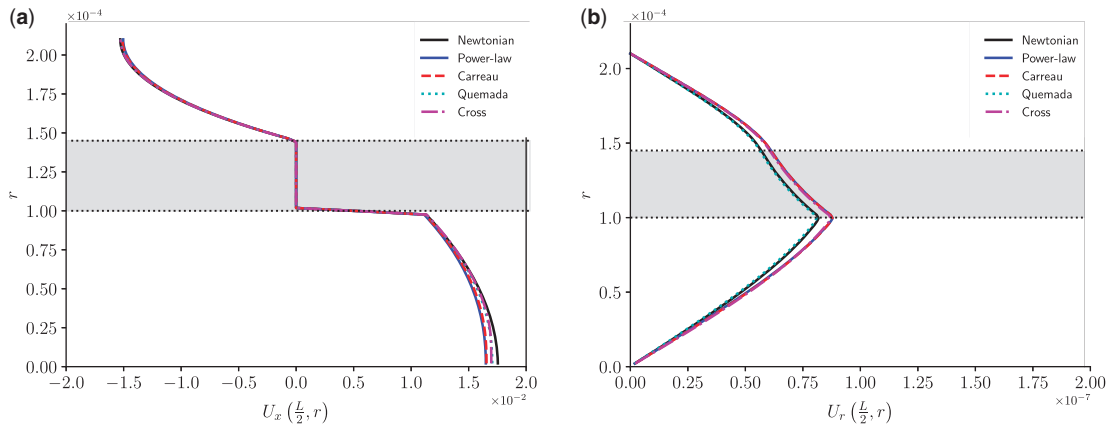
FIG. 5. Velocity profiles on the line $x = \dfrac{L}{2}$ corresponding to the geometry parameters in Table 2 (Set B) and the pressure boundary data optimized to match the flows in Table 4 (EX1). (a) Values (in $m \cdot s^{-1}$) of the longitudinal component of the velocity $U_x(\frac{L}{2}, r)$ for $r \in (0, R)$. (b) Values (in $m.s^{-1}$) of the radial component of the velocity $U_r(\frac{L}{2}, r)$ for $r \in (0, R)$.

in this paper, the values of the blood and the dialysate input and output pressures were chosen such that the blood and the dialysate flow rates match the values listed in Table 4. Therefore, the influence of the rheology is much less visible than in the case considered for Fig. 2 where the pressure data was the same for each rheology.

The longitudinal profiles of pressure in the blood and in the dialysate corresponding to a Newtonian model and for boundary pressure data optimized in order to minimize the functional $\mathcal{J}$ given by (3.13), are displayed in Fig. 6. We observe that these profiles are qualitatively different to the ones in Fig. 3(b) which correspond to pressure boundary data (3.2). More exactly, the pressure $p_{b,\text{out}}$ of the blood at the exit of the dialyzer is smaller than the pressure $p_{d,\text{in}}$ of the dialysate at the entrance of the dialyzer. This is surprising with respect to previous literature (see, for instance, Eloot *et al.*, 2002, 2006; Fasano & Farina, 2012) were it is often assumed that $p_{b,\text{out}} > p_{d,\text{in}}$ but, in the same time, is in complete agreement with the pressure values observed for a standard haemodialysis session and listed in Table 7.

4. Evolution of chemicals in blood and dialysate during dialysis

In this section we describe a model for the evolution of concentrations of several chemical components of blood and dialysate during a dialysis process. Since we are interested in the study of the calcium balance during haemodialysis using a citrate containing dialysate, we propose to use a transport–diffusion–reaction equation for a number of five chemical species described in Section 4.3. A similar model was employed for the study of the dynamic exchange of bicarbonate and the exchange of sodium during dialysis in Annan (2012a,b) and in Tilley (2009), respectively.

4.1 *Transport–diffusion process*

The solute concentration mechanism is coupled to the velocity field (U_x, U_r) is modelled by a convection–diffusion–reaction equation. More precisely, for any species (whose concentration is denoted by c_i,
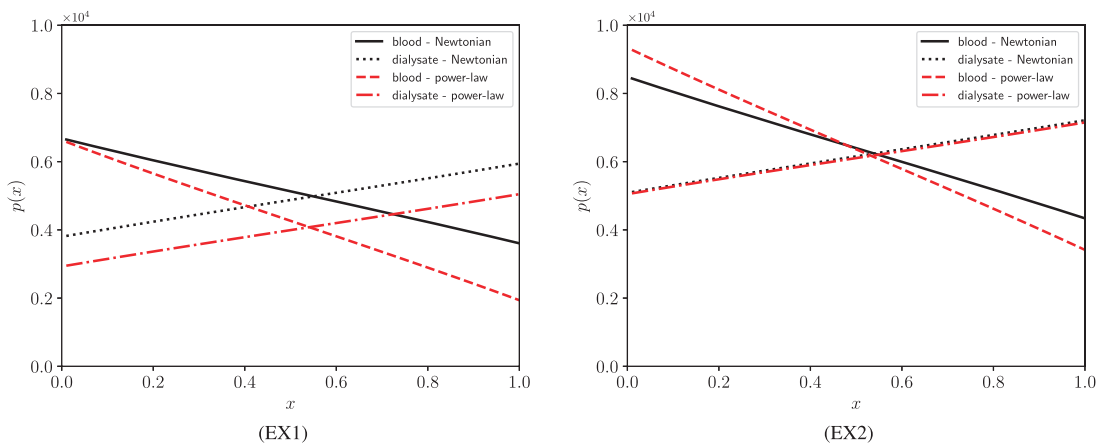
FIG. 6. Longitudinal profile of pressure in the blood and the dialysate corresponding to the geometry parameters in Table 2 (Set B) and the pressure boundary data optimized to match the flows in Table 4 (EX1) and (EX2).

$i = 1, ..., 5)$, we have, for every $(x, r) \in \Omega$ and $t > 0$,

$$\underbrace{\partial_t c_i}_{\text{transient}} + \underbrace{S_i(U_x \partial_x c_i + U_r \partial_r c_i)}_{\text{transport}} - \underbrace{\frac{1}{r}\partial_r(rD_i\partial_r c_i) - \partial_x(D_i\partial_x c_i)}_{\text{diffusion}} = \underbrace{F_i(c_1, ..., c_5)}_{\text{reaction}}. \tag{4.1}$$

The quantities D_i represent the diffusion coefficients ($m^2 \cdot s^{-1}$) and depend on each species i. The coefficients S_i are the so called sieving coefficients. A sieving coefficient equal to 1 corresponds to unhindered solute transport: it is naturally the case in blood or in dialysate domains. In the membrane, in order to take into account the size of the molecules, we impose that the sieving coefficients are equal to zero for large proteins like albumin (see Eloot *et al.*, 2006). The reaction source terms F_i model the interaction between different species. These terms will be precised later on in Section 4.3.

4.2 *Boundary conditions for the concentrations*

In order to complete the system (4.1) we need to impose some boundary conditions on the concentrations $(c_i)_{1 \le i \le 5}$. Therefore, we assume that each concentration c_i in the blood and in the dialysate at the entrance of the dialyzer is known. Indeed, since the dialysate composition is provided by its producer and the concentrations in the blood can be obtained by *a priori* measurements, this assumption is reasonable and translates into the following Dirichlet boundary conditions:

$$c_i = c_{i,\ell} \quad \text{on} \quad \Gamma_{\ell,b} \qquad \text{and} \qquad c_i = c_{i,r} \quad \text{on} \quad \Gamma_{r,d}. \tag{4.2}$$

On the remaining part of the boundary of Ω, the concentrations are unknown. A natural assumption is that the concentrations are constant in a neighbourhood of the boundary and in a direction perpendicular to the boundary. This hypothesis translates into the following Neumann boundary conditions:

$$\begin{cases} \partial_x c_i = 0 & \text{on} \quad \Gamma_{\ell,d} \cup \Gamma_{\ell,m} \cup \Gamma_{r,m} \cup \Gamma_{r,b}, \\ \partial_r c_i = 0 & \text{on} \quad \Gamma_b \cup \Gamma_d. \end{cases} \tag{4.3}$$

REMARK 4.1 For the system (4.1), the domain Ω is considered without the two interior boundaries Γ_{bm} and Γ_{md} separating the flow domains. This is possible because all the quantities appearing in (4.1) are defined over the entire domain Ω. Indeed, the velocity field (U_x, U_r) is defined everywhere even if it had been modelled initially using different equations for different flow domains. The diffusion coefficients D_i and the sieving coefficients S_i have different values for the blood, for the membrane and for the dialysate, but, even if these coefficients are discontinuous, the variational formulation associated to (4.1) is well-posed on the whole domain Ω.

4.3 *Biochemical reactions*

As mentioned before, we are interested in the complex formed by calcium, albumin and citrate. The equilibrium reactions for these species can produce the calcium–albumin as follows:

$$\text{calcium} + \text{albumin} \underset{k_2}{\overset{k_1}{\rightleftharpoons}} \text{calcium–albumin},$$
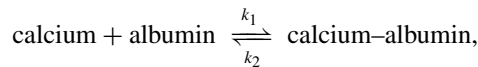
where the reaction rate constants are denoted by k_1 and k_2. We also note that albumin has 12 binding sites for calcium. The equilibrium reactions can also produce the calcium–citrate as follows:

$$\text{calcium} + \text{citrate} \underset{k_4}{\overset{k_3}{\rightleftharpoons}} \text{calcium–citrate},$$
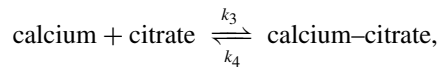
where the reaction rate constants are denoted by k_3 and k_4. Equilibrium constants were retrieved from literature data (Pedersen, 1971; Meyer, 1974; Silber & Rosen, 1976; Han *et al.*, 2013). Reaction rate constants k_i are more difficult to measure and fewer data are available. In this case, we assume that the studied chemical reactions follow a first order kinetics. The first rate constant is fixed arbitrarily (its magnitude is chosen according to the data available with similar reactions), the other constants being calculated such that their ratio is equal to the equilibrium constant. The values of the reaction constants used in this paper are given by:

$$k_1 = 1 \, \text{mol.m}^3 \cdot \text{s}^{-1}, \qquad k_2 = 10 \, \text{s}^{-1}, k_3 = 0.28 \, \text{mol} \cdot \text{m}^3 \cdot \text{s}^{-1}, \qquad k_4 = 0.15 \, \text{s}^{-1}.$$

Consequently, we consider five species whose concentrations c_i are listed below:

- c_1: concentration of calcium
- c_2: concentration of free albumin binding sites for calcium
- c_3: concentration of occupied albumin binding sites for calcium
- c_4: concentration of citrate
- c_5: concentration of calcium–citrate.

Since albumin molecules do not traverse the membrane, their corresponding sieving coefficients are given by

$$S_i(x) = \begin{cases} 1 & \text{if } x \in \Omega_b \cup \Omega_d \\ 0 & \text{if } x \in \Omega_m, \end{cases} \qquad \text{for } i \in \{2, 3\},$$

TABLE 5 *Typical values for the diffusion coefficients*

Name	Notation	Value ($m^2.s^{-1}$)
Reference diffusion	D	10^{-10}
Calcium diffusion	D_1	16.6×10^{-10}
Albumin diffusion	D_2 and D_3	0.877×10^{-10}
Citrate and calcium–citrate diffusion	D_4 and D_5	7.6×10^{-10}

TABLE 6 *Typical values (in $mol \cdot m^{-3}$) for the concentrations of the five considered chemical species in blood at the inlet of the hallow fibre (on $\Gamma_{\ell,b}$ and the concentrations for four dialysate fluids (on $\Gamma_{r,d}$)*

Name	Blood	Dialysate $\mathscr{D}_0$	Dialysate $\mathscr{D}_1$	Dialysate $\mathscr{D}_2$	Dialysate $\mathscr{D}_3$
Calcium (c_1)	1.2	1.5	0.981	1.11	0
Free albumin sites (c_2)	6.53	0	0	0	0
Calcium–albumin sites (c_3)	0.783	0	0	0	0
Citrate (c_4)	0.0307	0	0.281	0.26	0.8
Calcium–citrate (c_5)	0.0693	0	0.519	0.54	0

and all other sieving coefficients S_1, S_4 and S_5 are identically equal to one in Ω. Diffusion coefficients in the blood and the dialysate domains were assumed to be equal to diffusion coefficients in free water. Diffusion coefficients in free water were retrieved from literature data (Walters *et al.*, 1984; Southard *et al.*, 1991; Ribeiro *et al.*, 2008). When the diffusion coefficients in water at the temperature 310K were not available, they were calculated according to the Einstein relation. The diffusion coefficients in the membrane were assumed to be five times smaller than in water, as they can be measured for other solutes (see, for instance Eloot *et al.*, 2002). The values of the diffusion coefficients D_i at the temperature 310 K are gathered in Table 5.

Typical values for the concentrations in blood of the five chemical species in which we are interested are calculated according to the mass action law from data in the literature Pedersen (1971), Burtis *et al.* (2012) and Bauer *et al.* (2005) and are listed in the Table 6 (second column). We denote these concentration $(c_{i,\ell})_{1 \le i \le 5}$. We consider four dialysates having different concentrations of calcium and citrate. Their chemical compositions are listed in Table 6. Dialysate $\mathscr{D}_0$ is a classic dialysate, $\mathscr{D}_1$, $\mathscr{D}_2$ and $\mathscr{D}_3$ are citrate based dialysates with calcium concentrations of 1.5, 1.65 and 0 $mol \cdot m^{-3}$, respectively. These concentrations, denoted $(c_{i,r})_{1 \le i \le 5}$, appear as boundary conditions in (4.3).

With this notation, the reaction source terms F_i are described by the following relations:

$$F(c_1, ..., c_5) = \begin{pmatrix} k_2 c_3 + k_4 c_5 & - & k_1 c_1 c_2 - k_3 c_1 c_4 \\ k_2 c_3 & - & k_1 c_1 c_2 \\ -k_2 c_3 & + & k_1 c_1 c_2 \\ k_4 c_5 & - & k_3 c_1 c_4 \\ -k_4 c_5 & + & k_3 c_1 c_4 \end{pmatrix}.$$

4.4 Scaling procedure

Since the reference velocity in the blood (V) and the reference velocity in the membrane/dialysate (W) are different, we must choose a common reference velocity for the dialyzer. In practice, the complete velocity field (U_x, U_r) is written using the characteristic velocity V. More precisely, we introduce the non-dimensional velocity ($U_x^\star, U_r^\star$) such that

$$U_x = V\, U_x^\star \quad \text{and} \quad U_r = \varepsilon V\, U_r^\star.$$

Moreover, we need to introduce characteristic sizes for the concentrations c_i, for the diffusion coefficients D_i and for the reaction terms F_i (we choose k_2 as the reference reaction rate constant):

$$c_i = C\, c_i^\star, \quad D_i = D\, D_i^\star, \quad F_i = k_2\, C\, F_i^\star.$$

In the rescaled domain, and, therefore, for every $(x^\star, r^\star) \in \omega$ and $t^\star > 0$, (4.1) becomes:

$$\partial_{t^\star} c_i^\star + S_i \left(U_x^\star \partial_{x^\star} c_i^\star + U_r^\star \partial_{r^\star} c_i^\star \right) - \frac{1}{\mathscr{P}e} \frac{1}{r^\star} \partial_{r^\star} (r^\star D_i \partial_{r^\star} c_i^\star) - \frac{\varepsilon^2}{\mathscr{P}e} \partial_{x^\star} (D_i \partial_{x^\star} c_i^\star) = \frac{1}{\mathscr{F}d} F_i^\star(c_1^\star, ..., c_5^\star), \quad (4.4)$$

and the reaction source term is given by

$$F^\star(c_1^\star, ..., c_5^\star) = \begin{pmatrix} c_3^\star + \delta_2 c_5^\star & - & \delta_1 c_1^\star c_2^\star - \delta_3 c_1^\star c_4^\star \\ c_3^\star & - & \delta_1 c_1^\star c_2^\star \\ -c_3^\star & + & \delta_1 c_1^\star c_2^\star \\ \delta_2 c_5^\star & - & \delta_3 c_1^\star c_4^\star \\ -\delta_2 c_5^\star & + & \delta_3 c_1^\star c_4^\star \end{pmatrix}.$$

Note that we have introduced five supplementary non-dimensional numbers:

$$\mathscr{P}e = \frac{R^2\, V}{L\, D}, \qquad \mathscr{F}d = \frac{V}{L\, k_2}, \qquad \delta_1 = \frac{k_1\, C}{k_2}, \qquad \delta_2 = \frac{k_4}{k_2} \quad \text{and} \quad \delta_3 = \frac{k_3\, C}{k_2}.$$

Using the parameters given in Table 2 Set B, Table 5, Table 6 and input pressures optimized in order to match the flow rates in Table 4 EX1, the following values are obtained for the model parameters:

$$\mathscr{P}e \approx 588, \qquad \mathscr{F}d \approx 0.133, \qquad \delta_1 = 10^{-1}, \qquad \delta_2 = 1.5 \times 10^{-2} \quad \text{and} \quad \delta_3 = 2.8 \times 10^{-2}.$$

Even if the Péclet's number $\mathscr{P}e$ is of order of $1/\varepsilon$ we prefer to keep the term $\frac{1}{\mathscr{P}e} \frac{1}{r^\star} \partial_{r^\star} (r^\star D_i \partial_{r^\star} c_i^\star)$ in (4.4). In fact, this term has a regularizing effect for the solutions $(c_i)_{1 \leq i \leq 5}$ and this is important particularly for discontinuous initial concentrations.

Finally, the boundary conditions become

$$\begin{cases} \partial_{x^\star} c_i^\star = 0 & \text{on} \quad \gamma_{\ell,d} \cup \gamma_{\ell,m} \cup \gamma_{r,m} \cup \gamma_{r,b}, \\ \partial_{r^\star} c_i^\star = 0 & \text{on} \quad \gamma_b \cup \gamma_d, \\ c_i^\star = c_{i,\ell}/C & \text{on} \quad \gamma_{\ell,b}, \\ c_i^\star = c_{i,r}/C & \text{on} \quad \gamma_{r,d}. \end{cases}$$

We complete this system with the following initial conditions:

$$c_i^\star(x^\star, 0) = c_i^{0,\star}(x^\star) = \begin{cases} c_{i,\ell}/C & \text{if } x^\star \in \omega_b, \\ c_{i,r}/C & \text{if } x^\star \in \omega_m \cup \omega_d, \end{cases} \quad \text{for } i \in \{1, 2, 3, 4, 5\}.$$

4.5 *Variational formulation and numerical approach*

In order to numerically solve (4.4), we consider its variational formulation detailed at the end of Appendix B. We use an implicit one step discretization scheme in time and the finite elements method for the space discretization. Moreover, in order to obtain a faster numerical solver, we compute one concentration $c_i^\star$ at a time, replacing the unavailable concentrations at the current time step by their values at the previous time step. For a given time $t^\star > 0$, concentrations $c_i^\star(t^\star, x^\star, r^\star)$ are represented using $\mathbb{P}_1$ finite elements and `FreeFem++` is used for the numerical implementation.

For every time $t^\star > 0$, we denote $E(t^\star)$ the following quantity associated to the evolution in time of concentrations $c_i^\star(t^\star, \cdot, \cdot)$ and defined by

$$E(t^\star) = \left(\sum_{i=1}^{5} \iint_\omega r^\star \left| c_i^\star(t^\star, x^\star, r^\star) \right|^2 dx^\star dr^\star \right)^{\frac{1}{2}} \quad \text{for every } t^\star > 0. \tag{4.5}$$

Let $E'(t^\star)$ be the derivative with respect to the time $t^\star$ of the function E. It is easy to remark that when concentrations $(c_i^\star(t^\star))_{1 \leq i \leq 5}$ approach a stationary solution, $E'(t^\star)$ will be close to zero. For all the simulations in Section 5, we choose a time interval $(0, T^\star)$ where we compute the concentrations $c_i^\star$, such that $E'(T^\star) \leq 10^{-4}$.

5. Numerical experiments

Pressure measurements were effectuated on an APS18 dialyzer for a dialysate input flux of $500 \, \text{ml} \cdot \text{min}^{-1}$ and an ultra-filtration flux equal to $10 \, \text{ml} \cdot \text{min}^{-1}$. Pressure values were recorded, using pressure sensors situated at the level of the input and of the exit of the blood and of the dialysate tubes respectively. The values for two different input blood fluxes are listed in Table 7. The pressures at the level of the hollow fibre (our computation domain) were numerically computed by the optimization method proposed in the Section 3.5.2, such that the corresponding flows are the ones indicated in Table 4.

The APS18 dialyzer has a diameter of 4.2 cm and it is composed of a number of $N = 10^4$ fibres, with an inner channel having a radius of $10^{-4} \, \text{m}$ and a wall thickness of hollow fibres of $0.45 \times 10^{-4} \, \text{m}$. The length of such a dialyzer is 33 cm. These values are exactly the same as those listed in Table 2 Set B.

TABLE 7 *Values of input and output pressures (in mmHg) for a dialysate flux of* $500 \, \text{ml} \cdot \text{min}^{-1}$ *and an ultrafiltration flux of* $10 \, \text{ml} \cdot \text{min}^{-1}$

	Input blood flux	Blood input pressure	Blood output pressure	Dialysate input pressure	Dialysate output pressure
(EX1)	$300 \, \text{ml} \cdot \text{min}^{-1}$	200	110	200	95
(EX2)	$400 \, \text{ml} \cdot \text{min}^{-1}$	276	164	262	58
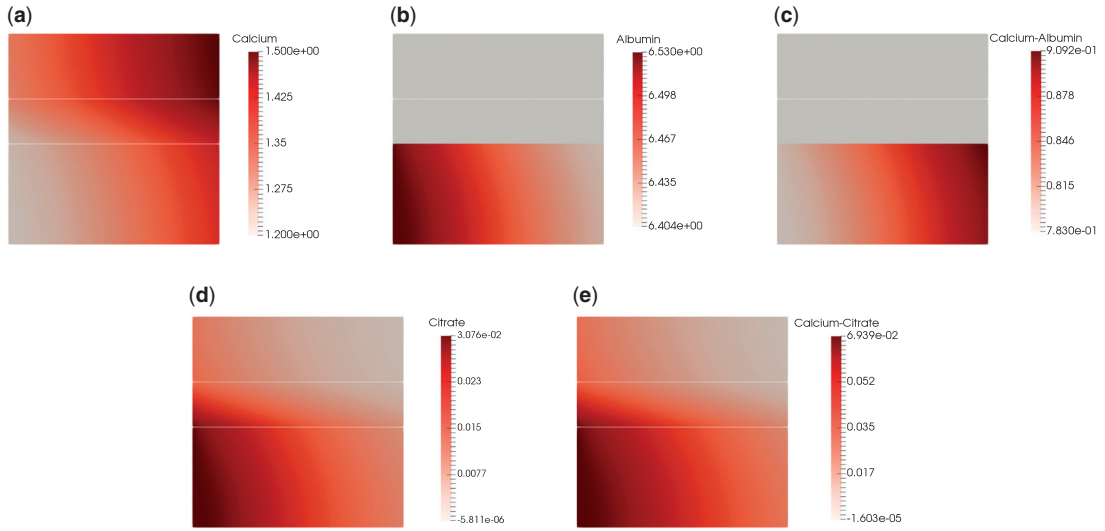
FIG. 7. Concentrations c_i (in mol $\cdot$ m^{-3} or, equivalently, in mmol$\cdot$l^{-1}) in the domain ω at a non-dimensional time T^* corresponding to approximately 300 s, for (EX1) and dialysate $\mathscr{D}_0$: (a) calcium, (b) free albumin binding sites for calcium, (c) calcium-albumin sites, (d) citrate and (e) calcium–citrate.

5.1 Concentrations for blood modelled as a Newtonian fluid

The spatial concentrations for all considered species at a (no-dimensional) time $T^\star$ such that $E'(T^\star) < 10^{-4}$, that were obtained for the flows given by (EX1), are displayed in Fig. 7. More precisely, for all the numerical experiments, we choose $T^\star = 300T$, which corresponds to a real time of 300 s and verifies the condition $E'(T^\star) < 10^{-4}$. This value of $T^\star$ is a good compromise between the computational cost and the reach of the equilibrium in the chemical reactions.

In Fig. 7, we remark that the concentrations computed by the model are smooth enough and that the imposed boundary conditions are well satisfied. We also remark an increase of the concentration of calcium and of calcium–albumin sites in the blood at the exit of the dialyzer. Consequently, the amount of calcium in the dialysate fluid is smaller in the rejected fluid than it was at the dialyzer input. In the same time, a part of the citrate and of the calcium–citrate passes from the blood into the dialysate.

In order to analyse the evolution of the concentration for the five chemical species considered here, we define the mean concentrations in the output blood $\overline{c}_i(t)$ at the time t by

$$\overline{c}_i(t) = \frac{2R^2}{R_1^2} \int_0^{\frac{R_1}{R}} r\, c_i(t, 1, r)\, \mathrm{d}r.$$

In Fig. 8 we can follow the evolution in time of the concentration $\overline{c}_1(t)$ of free calcium in the blood at the dialyzer's outlet for a velocity field computed in order to fulfil the flow rates in Table 4 (EX1) and two different blood rheologies: Newtonian fluid and a non-Newtonian fluid (the power-low model). The blood composition at the dialyzer's inlet and the four dialysates $\mathscr{D}_0$, $\mathscr{D}_1$, $\mathscr{D}_2$ and $\mathscr{D}_3$ are described in Table 6. Remark that, at $T^\star = 300T$, the value $E'(T^\star)$ is relatively small and the mean concentrations of free calcium in the blood at the exit of dialyzer reached their stationary values. A similar behaviour was observed for all the other chemical species considered by the model.
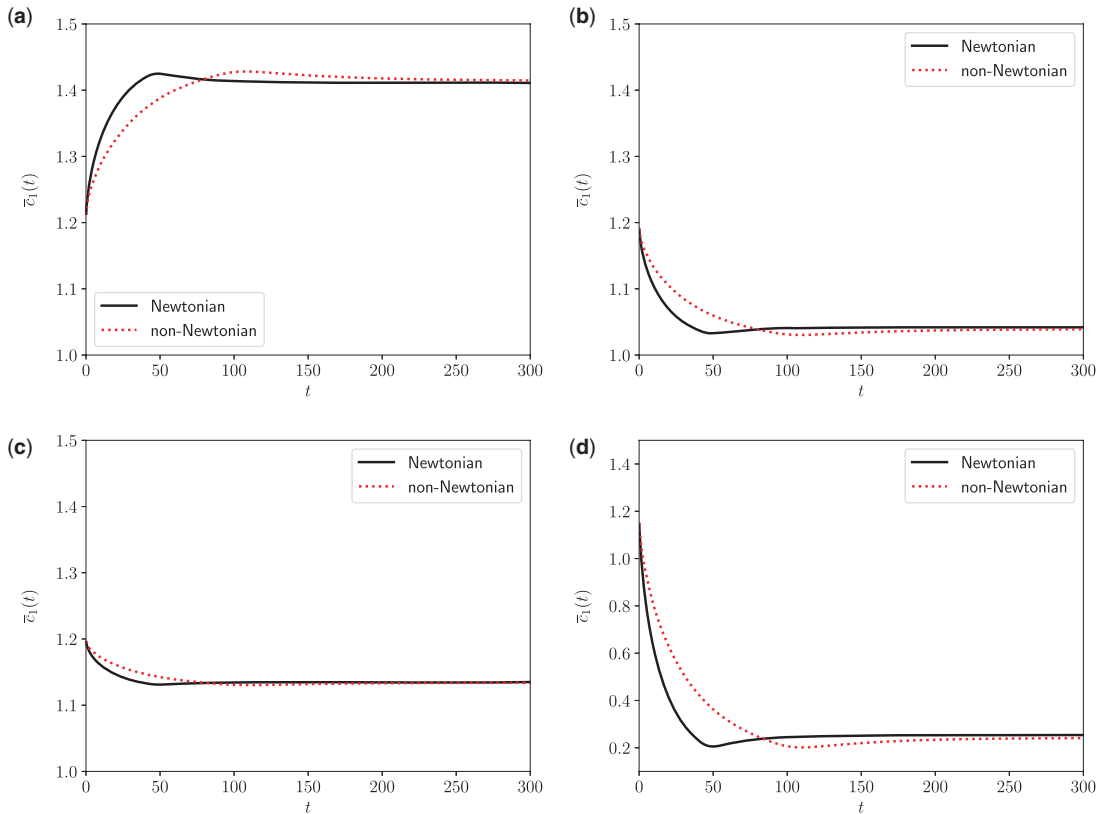
FIG. 8. Evolution of the concentration $\bar{c}_1(t)$ (in mol $\cdot$ m^{-3} or, equivalently, in mmol $\cdot$ l^{-1}) of the free calcium in the blood at the exit of the dialyzer for dialysate fluids described in Table 6. (a) Dialysate $\mathscr{D}_0$, (b) Dialysate $\mathscr{D}_1$, (c) Dialysate $\mathscr{D}_2$ and (d) Dialysate $\mathscr{D}_3$.

The results illustrated in Fig. 8 are in complete agreement with what is expected from a chemical point of view, the concentration of total calcium in the blood tending to a concentration situated between the initial concentrations in the blood and the dialysate. Moreover, for citrate containing dialysates we observe an increase of 10^{-1}mmol $\cdot$ l^{-1} of the total calcium in the blood for dialysate $\mathscr{D}_2$ with respect to dialysate $\mathscr{D}_1$.

The spatial distribution of the concentration of calcium corresponding to the final time associated to the simulations illustrated in Fig. 8, are displayed in Fig. 9. More precisely, we display the spatial distribution of the calcium concentration c_1 associated to the flow-rates (EX1) and the boundary concentrations in Tables 6 at the time T^* corresponding to a real time equal to 300 s.

In all four graphics depicted in Fig. 9 we observe that the radial variation of the calcium concentration in the blood and the dialysate is less important than in the membrane. Therefore, the concentration of calcium at the interface blood/membrane is close to the mean concentration of calcium in the blood for every longitudinal position x.

In order to check whether the free calcium concentration was sufficiently decreased in the dialyzer to have an anticoagulant effect, we computed the longitudinal profiles of the concentration of free calcium at the interface blood/membrane. Calculation were made for both flows (EX1) and (EX2). Results are
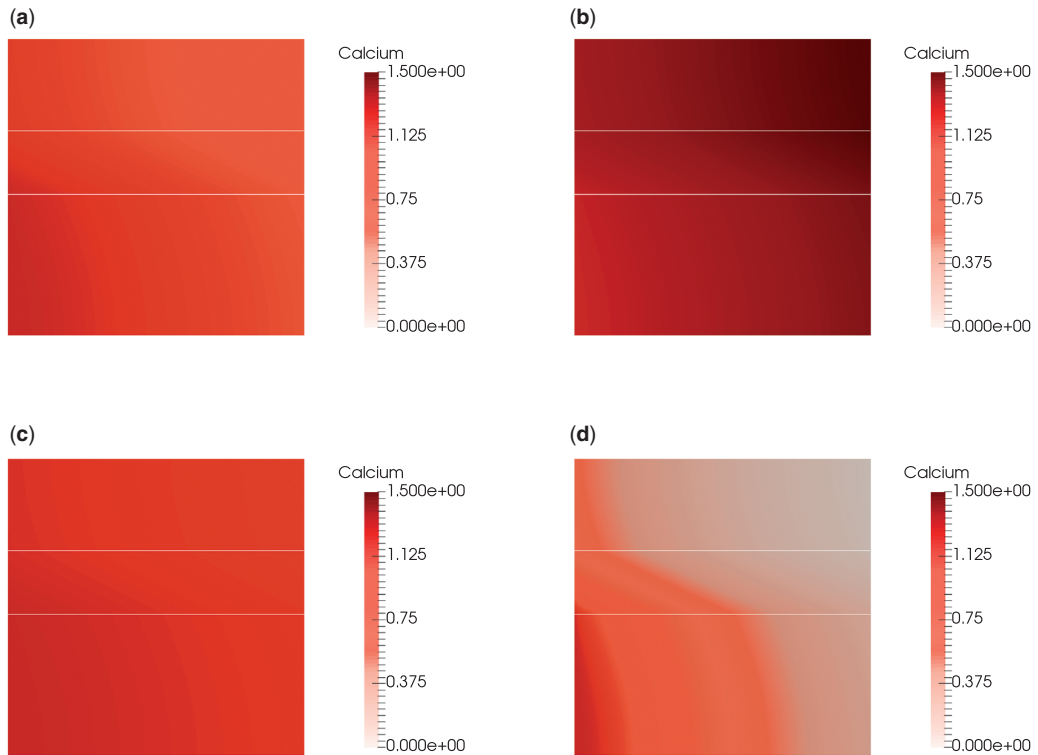
FIG. 9. Spatial distribution of the concentration c_1 (in mol $\cdot$ m^{-3} or, equivalently, in mmol $\cdot$ l^{-1}) of the free calcium at the time 300 s for the dialysate fluids described in Table 6. (a) Dialysate $\mathscr{D}_0$, (b) Dialysate $\mathscr{D}_1$, (c) Dialysate $\mathscr{D}_2$ and (d) Dialysate $\mathscr{D}_3$.

shown in Fig. 10. While the concentration of free calcium increases with the dialysate $\mathscr{D}_0$, it decreases with the dialysates $\mathscr{D}_1$ and $\mathscr{D}_2$. However, it remains greater than 1 mmol $\cdot$ l^{-1} throughout the dialyzer. With dialysate $\mathscr{D}_3$ the decrease of calcium concentration is more marked, passing below 0.5 mmol $\cdot$ l^{-1} along the distal third of the dialyzer.

A quantity of clinical interest is the concentration of total calcium in the blood at the dialyzer's outlet. Indeed, being given the total calcium at the inlet of the dialyzer, the blood and the ultrafiltration flows, it is possible to calculate the transfer of calcium between the blood of the patient and the dialysate (Sargent & Gotch, 1989). In Fig. 11 we display the evolution of the concentration of total calcium $\bar{c}(t) = \bar{c}_1(t) + \bar{c}_3(t) + \bar{c}_5(t)$ in the blood at the exit of the dialyzer. We observe that when using a citrate dialysate, the transfer of calcium from the dialysate to the blood is less important. For the same calcium concentration in the dialysate at the inlet of the dialyzer, the total calcium concentration in the blood at the outlet is lesser when the dialysate contains citrate (dyalysate $\mathscr{D}_1$ with respect to dialysate $\mathscr{D}_0$). Finally, for the dialysate $\mathscr{D}_3$, which contains the same amount of citrate as $\mathscr{D}_1$ and $\mathscr{D}_2$ and no calcium, the total concentration of calcium in the blood at the dialyzer's outlet drops under 0.8 mmol $\cdot$ l^{-1}. Thus, given the blood flow $Q_{b,\text{out}}$, we can easily compute the quantity of calcium c^i to be infused in the blood at the dialyzer's outlet, such that the total concentration of calcium in the dialyzed blood will be equal to c^{target}:

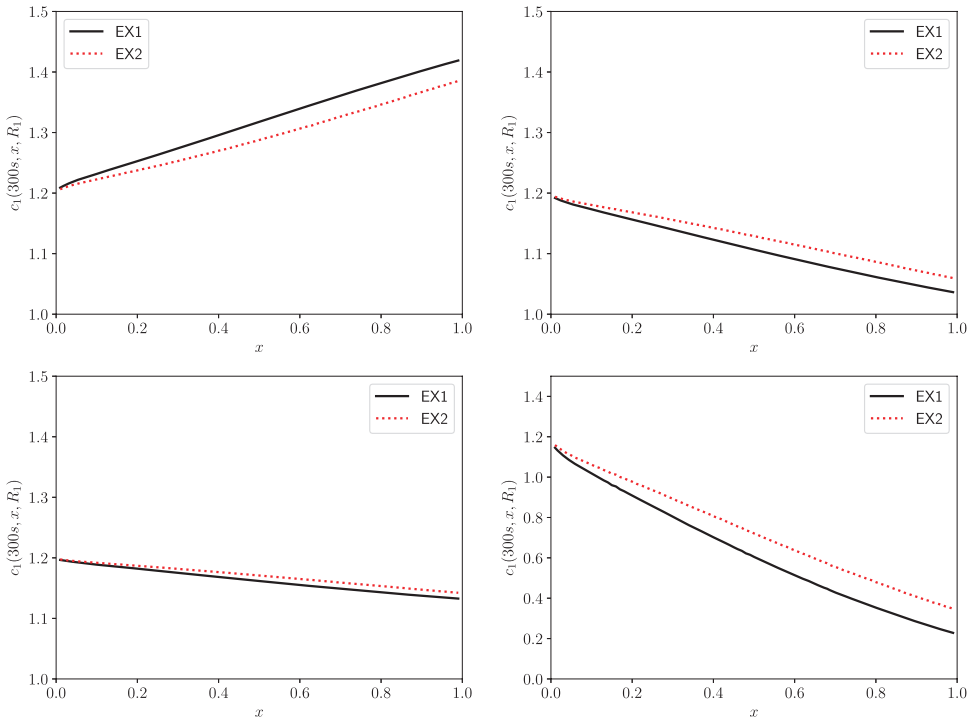$$c^i = Q_{b,\text{out}} \left(c^{\text{target}} - \bar{c}(T^*) \right).$$

FIG. 10. Longitudinal distribution of the concentration $\overline{c}_1(t)$ (in mol·m^{-3} or, equivalently, in mmol·l^{-1}) of free calcium in the blood at the blood/membrane interface at time 300 s for dialysate fluids described in Table 6. Left-top: dialysate $\mathscr{D}_0$. Right-top: dialysate $\mathscr{D}_1$. Left-bottom: dialysate $\mathscr{D}_2$. Right-bottom: Dialysate $\mathscr{D}_3$.
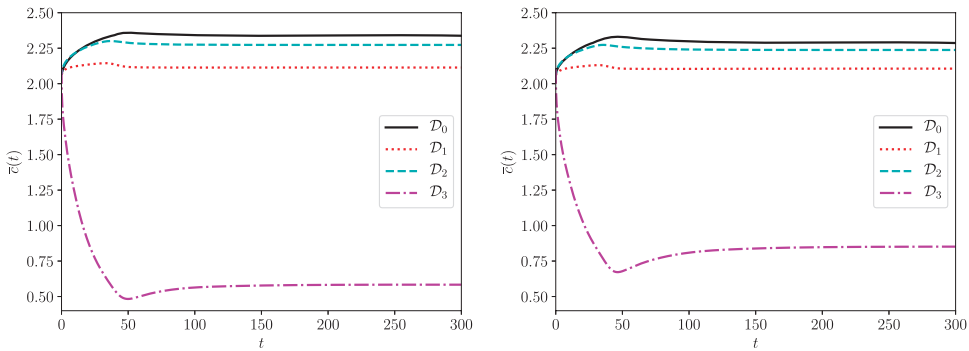

FIG. 11. Evolution of the concentration of the total calcium in the blood at the exit of the dialyzer for flow data in Table 6 and dialysates $\mathscr{D}_0$, $\mathscr{D}_1$, $\mathscr{D}_2$ and $\mathscr{D}_3$. Left: (EX1). Right: (EX2).

5.2 *Concentrations for blood modelled as a non-Newtonian fluid*

In this section the velocity field (U_x, U_r) driving the convective part in (4.1) is computed using a non-Newtonian model for the blood. Since we are interested in the influence of the blood's rheology on the
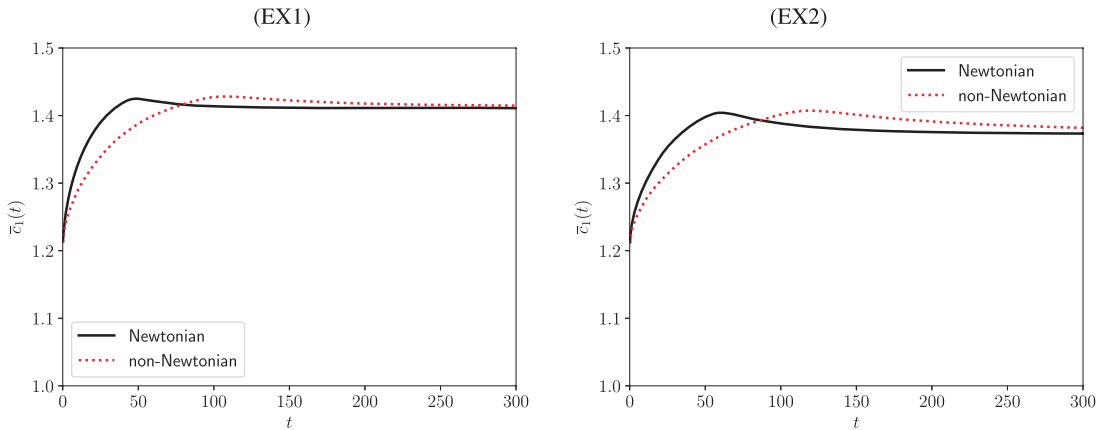
FIG. 12. Mean concentration of free calcium $\bar{c}_1$ (in mol $\cdot$ m^{-3} or, equivalently, in mmol $\cdot$ l^{-1}) in blood at the exit of the dialyzer for Newtonian and non-Newtonian (power-law) blood flows for (EX1) and (EX2).

evolution of the concentrations for the five chemical species listed at the beginning of this section, we only consider here the power-law model which seems to provide results which are the least similar to the Newtonian case.

As in the Newtonian case, we stop the numerical experiments at the time $T^\star = 300\,T$ for which the value $E'(T^\star)$ is acceptably small. We recall that this time corresponds to 300 s.

In order to compare the evolution of concentrations for the Newtonian and non-Newtonian blood flows, Fig. 12 displays the evolution of the concentration of free calcium in blood at the exit of the dialyzer for the first five minutes of the dialysis. Small differences can be observed for small values of the time t, the concentration $\bar{c}_1$ arriving at the same stationary solution for both types of flows. These differences are due to the different values of the reference velocity V for each rheology, and, hence, are due to the dependence of the reference time T on the rheology. Nevertheless, for large values of the time T we remark a very small influence of the blood's rheology on the concentrations of the five chemical species considered by the model.

In conclusion, since the fluid system is easier to solve in the linear case and since the rheology seems to have only a small influence on the evolution of the concentrations of the chemical species in the blood and in the dialysate considered here, we propose to use the Newtonian model for the blood in a future studies of the evolution of chemical species during dialysis.

6. Conclusion and perspectives

The modelling yielded two interesting results for clinical practice.

First, the decrease in free calcium concentration in the blood is insufficient to explain the anticoagulant effect of citrate-containing dialysate. With a citrate-free dialysate, the free calcium concentration of the blood increases between the inlet and the outlet of the dialyzer. Conversely, with a citrate-containing dialysate, the free calcium concentration decreases (see Fig. 10).

However, on contact with the membrane the free calcium concentration remains higher than $0.4\,\text{mmol} \cdot \text{l}^{-1}$. Only a citrate based dialysate without calcium can decrease free calcium concentration at the blood membrane interface low enough to inhibit blood coagulation in the distal third of the

dialyzer. This segment is the most at risk of blood clotting due to haemoconcentration. The modest anti-coagulant effect of calcium and citrate containing dialysate could be related to its inhibitory effect on the complement system (Huang *et al.*, 2014).

Second, for a given calcium concentration in the blood at the inlet of the dialyzer, the total calcium concentration in the blood at the outlet is lower when the dialysate contains citrate (see Fig. 11). The decrease in calcium returning to the patient could explain the increased risk of secondary hyperparathyroidism in patients with citrate dialysate (Molina Nunez *et al.*, 2015). When the quantity of calcium is augmented in a citrate containing dialysate we can hope to have the same concentration of calcium in the blood at the dialyzer's inlet and dialyzer's outlet. This is almost the case for dialysate $\mathscr{D}_2$. The precise concentration of calcium in the dialysate needed to achieve a desired concentration of calcium in the blood at the dialyzer's outlet could be computed using an optimization strategy and will make the object of a future work. Our modelling predicts that a citrate dialysate containing $1.65 \, \text{mmol} \cdot \text{l}^{-1}$ of calcium provides a calcium concentration in the blood at the outlet of the dialyzer equivalent to that obtained with a citrate-free dialysate containing $1.5 \, \text{mmol} \cdot \text{l}^{-1}$ of calcium. This is an important issue to be considered in clinical practice since calcium balance acts directly on bone and mineral disorders in haemodialysis patients. Moreover in the case of a calcium free citrate containing dialysate, to avoid undesirable events due to the re-injection of a calcium-poor blood into the patient our model makes it possible to calculate the amount of calcium to be injected into the blood at the exit of the dialyzer.

Concerning the mathematical model, we observed that the choice of blood rheology had little effect on the evolution of the mean concentrations at the dialyzer outlet or on the concentrations at the level of the membrane. A possible explanation is that we applied an optimization algorithm to choose the boundary conditions of the blood and dialysate pressures at the inlet and outlet of a hollow fibre such that the corresponding flow rates match the flow rates measured on the dialyzer. This method allowed us to choose standard boundary conditions for the fluid model. Hence, once the boundary data on pressure are computed, the blood can be assumed to be a Newtonian fluid and velocity fields can be computed numerically or even explicitly (Fasano & Farina, 2012). The velocity field obtained by solving the fluid model by a finite element method acts as an input for the convective part in the convection–diffusion–reaction system that models the evolution of five chemical species present in the blood and in the dialysate fluid. Our work was focused on the concentration of calcium ions and so, we considered only five chemical species corresponding to the complex formed by calcium, albumin and citrate. But, the model can be easily enriched to take into account a larger number of chemical species and this will be the subject of a future work.

Our study has several limitations. First, the rate constants of the chemical reactions used to model the interaction between calcium, citrate and albumin do not take into account the changes caused by possible variations in the pH of the dialysate and the blood. However, at least for the citrate and calcium reaction, it appears that the change in pH has no influence on the equilibrium constants. Chemical equilibrium is reached much more quickly than other physical phenomena involved. Thus, the exact value of the rate constants has little significance provided that their ratio (equilibrium constant) is right (Musvoto *et al.*, 2000). Also, we did not take into account the phenomenon of electrical migration. The different ion diffusion rates lead to the appearance of an electric field. However, this mechanism plays a minor role in the solute flux in the dialyzer, particularly with the new polysulfone membranes (Yamamoto *et al.*, 2010). Finally, our model does not take into account that oncotic pressure depends on the concentrations of solutes and is assumed to variate non-linearly with respect to the longitudinal variable. To take into account the dependence of the oncotic pressure on blood solute concentration we should have to devise a model with a stronger coupling between the equation describing the fluid flows and those modelling the transport of solutes. This will be the subject of a future work.

A greater knowledge of calcium ion concentrations in the dialyzer would help improve the management of haemodialysis patients. Modelling offers the opportunity to predict these data, which are not easily measurable. The partial differential equation model and the finite element method used in our work offer the possibility to predict diffusion and convection and also the chemical reactions between several solutes. This method could be adapted to predict and optimize the purification of uremic toxins bound to albumin.

Acknowledgments

Funding

REFERENCES

ANNAN, K. (2012a) Finite volume scheme for double convection-diffusion exchange of solutes in bicarbonate high-flux hollow-fiber dialyzer therapy. *Comput. Math. Methods Med.*, **2012**, 1–16.

ANNAN, K. (2012b) Mathematical modeling of the dynamic exchange of solutes during bicarbonate dialysis. *Math. Comput. Model.*, **55**, 1691–1704.

BAUER, E., DERFLER, K., JOUKHADAR, C. & DRUML, W. (2005) Citrate kinetics in patients receiving long-term hemodialysis therapy. *Am. J. Kidney Dis.*, **46**, 903–907.

BECK, S. C., UPHOFF, S., LANGER, S. C. & KRAFCZYK, M. (2014) Sensitivity of the slip rate coefficient in fluid flow poroelastic coupling conditions. *PAMM*, **14**, 699–700.

BURTIS, C. A., ASHWOOD, E. R. & BRUNS, D. E. (2012) *Tietz Textbook of Clinical Chemistry and Molecular Diagnostics*. Louis, USA: Elsevier Health Sciences.

DAVENPORT, A. (2011) What are the anticoagulation options for intermittent hemodialysis? *Nat. Rev. Nephrol.*, **7**, 499–508.

ELOOT, S., DE WACHTER, D., TRICHT, I. V. & VERDONCK, P. (2002) Computational flow modeling in hollow-fiber dialyzers. *Artif. Organs*, **26**, 590–599.

ELOOT, S., VIERENDEELS, J. & VERDONCK, P. (2006) Optimisation of solute transport in dialysers using a three-dimensional finite volume model. *Comput. Methods Biomech. Biomed. Eng.*, **9**, 363–370.

FASANO, A. & FARINA, A. (2012) Modeling high flux hollow fibers dialyzers. *Discrete Contin. Dyn. Syst. Ser. B*, **17**, 1903–1937.

GLOWINSKI, R. (2003) Finite element methods for incompressible viscous flow. *Handbook of Numerical Analysis* (G. Ciarlet Philipe & J. L. Lions eds), vol. IX. Handbook of Numerical Analysis, IX. Amsterdam, North-Holland, pp. 3–1176.

GOTCH, F., KOTANKO, P., HANDELMAN, G. & LEVIN, N. (2007) A kinetic model of calcium mass balance during dialysis therapy. *Blood Purif*, **25**, 139–149.

Kidney Disease: Improving Global Outcomes (KDIGO) CKD-MBD Work Group *et al.* KDIGO clinical practice guideline for the diagnosis, evaluation, prevention, and treatment of chronic kidney disease-mineral and bone disorder (ckd-mbd). *Kidney Int. Suppl.*, **76** (Supplement 113):S1, 2009.

HAN, J., XUE, J.-F., XU, M., GUI, B.-S., KUANG, L. & OUYANG, J.-M. (2013) Coordination dynamics and coordination mechanism of a new type of anticoagulant diethyl citrate with Ca2. *Bioinorgan. Chem. Appl.*, **2013**, 1–8.

HECHT, F. (2012) New development in FreeFem++. *J. Numer. Math.*, **20** 251–265.

HIMMELFARB, J. & ALP IKIZLER, T. (2010) Hemodialysis. *New Engl. J. Med.*, **363**, 1833–1845.

HUANG, S., SANDHOLM, K., JONSSON, N., NILSSON, A., WIESLANDER, A., GRUNDSTRM, G., HANCOCK, V. & EKDAHL, K. N. (2014) Low concentrations of citrate reduce complement and granulocyte activation in vitro in human blood. *Clin. Kidney J.*, **8**, 31–37.

JAMES, M. F. M. & ROCHE, A. M. (2004) Dose-response relationship between plasma ionized calcium concentration and thrombelastography. *J. Cardiothorac. Vasc. Anesth.*, **18**, 581–586.

KEDEM, O. & KATCHALSKY, A. (1958) Thermodynamic analysis of the permeability of biological membranes to non-electrolytes. *Biochim. Biophys. Acta*, **27**, 229–246.

KEENER, J. P. & SNEYD, J. *Mathematical Physiology*., vol. 1. New York: Springer, 1998.

KOSSMANN, R. J., GONZALES, A., CALLAN, R. & AHMAD, S. (2009) Increased efficiency of hemodialysis with citrate dialysate: a prospective controlled study. *Clin. J. Am. Soc. Nephrol.*, **4**, 1459–1464.

LEGALLAIS, C., CATAPANO, G., VON HARTEN, B. & BAURMEISTER, U. (2000) A theoretical model to predict the in vitro performance of hemodiafilters. *J. Membr. Sci.*, **168**, 3–15.

MEYER, J. L. (1974) Formation constants for interaction of citrate with calcium and magnesium ions. *Anal. Biochem.*, **62**, 295–300.

MOLINA NUNEZ, M., DE ALARCÓN, R., ROCA, S., ÁLVAREZ, G., ROS, M. S., JIMENO, C., BUCALO, L., VILLEGAS, I. & GARCíA, M. A. (2015) Citrate versus acetate-based dialysate in on-line haemodiafiltration. a prospective cross-over study. *Blood Purification*. **39**, 181–187.

MAMUN MOLLA, M. & PAUL, M. C. (2012) LES of non-newtonian physiological blood flow in a model of arterial stenosis. *Med. Eng. Phys.*, **34**, 1079–1087.

MUSVOTO, E. V., WENTZEL, M. C., LOEWENTHAL, R. E. & EKAMA, G. A. (2000) Integrated chemical physical processes modelling development of a kinetic-based model for mixed weak acid/base systems. *Water Res.*, **34**, 1857–1867.

NEALE, G. & NADER, W. (1974) Practical significance of Brinkman's extension of Darcy's law: coupled parallel flows within a channel and a bounding porous medium. *Can. J. Chem. Eng.*, **52**, 475–478.

PEDERSEN, KO. (1971) Binding of calcium to serum albumin I. Stoichiometry and intrinsic association constant at physiological pH ionic strength, and temperature. *Scand. J. Clin. Lab. Invest.*, **28**, 459–469.

RIBEIRO, A. C. F., BARROS, M. C. F., TELES, A. S. N., VALENTE, A. J. M., LOBO, V. M. M., SOBRAL, A. J. F. N. & ESTESO, M. A. (2008) Diffusion coefficients and electrical conductivities for calcium chloride aqueous solutions at 298.15 k and 310.15 k. *Electrochim. Acta*., **54**, 192–196.

SARGENT, J. & GOTCH, F. Principles and biophysics of dialysis. *Replacement of Renal Function by Dialysis*. (J.F. Maher, ed.) Netherlands: Springer, pp. 87–143, 1989.

SILBER, H. B. & ROSEN, J. (1976) Gadolinium and calcium binding to bovine serum albumin. *J. Inorgan. Nuclear Chem.*, **38**, 1415–1419.

SOUTHARD, M. Z., DIAS, L. J., HIMMELSTEIN, K. J. & STELLA, V. J. (1991) Experimental determinations of diffusion coefficients in dilute aqueous solution using the method of hydrodynamic stability. *Pharm. Res.*, **8** 1489–1494.

THIJSSEN, S., KRUSE, A., RAIMANN, J., BHALANI, V. LEVIN, N. W. & KOTANKO, P. (2010) A mathematical model of regional citrate anticoagulation in hemodialysis. *Blood Purif.*, **29**, 197–203.

TILLEY, BS. (2009) Sodium flux during haemodialysis. *Proceedings of the OCCAM–Fields–MITACS Biomedical Problem Solving Workshop* (G. M. Lewis ed.).

VILLARROEL, F., KLEIN, E. & HOLLAND, F. (1977) Solute flux in hemodialysis and hemofiltration membranes. *ASAIO J.*, **23**, 225–232.

WALTERS, R. R., GRAHAM, J. F., MOORE, R. M. & ANDERSON, D. J. (1984) Protein diffusion coefficient measurements by laminar flow analysis: method and applications. *Anal. Biochem.*, **140**, 190–195.

YAMAMOTO, K., OGAWA, T., MATSUDA, M., IINO, A., YAKUSHIJI, T., MIYASAKA, T. & SAKAI, K. (2010) Membrane potential and charge density of hollow-fiber dialysis membranes. *J. Membr. Sci.*, **355**, 182–185.

Appendix A. Dimensionless equations

The goal of this first appendix is to present the non-dimensional form of the equations describing the hydrodynamic flow (see Section 3.1). More precisely, we rewrite all the equations introduced in this

section using the changes of variable given in Section 3.2.2. Consequently, all quantities should be marked with an asterisk but here we drop the asterisks for the sake of clarity.

For every $t > 0$ and $(x, r) \in \omega_b$, the dimensionless equations governing the blood flow read as follows (see Section 3.1.1 for the dimensional form of these equations):

$$
\begin{cases}
\varepsilon \mathscr{R}e\left(\partial_t v_x + v_x \partial_x v_x + \dfrac{1}{r} v_r \partial_r (r v_x)\right) = -\partial_x p_b + 2\varepsilon^2 \partial_x\left(\widetilde{G}(\dot\gamma)\, \partial_x v_x\right) + \dfrac{1}{r} \partial_r\left(r\, \widetilde{G}(\dot\gamma)\, (\partial_r v_x + \varepsilon^2 \partial_x v_r)\right), \\[2mm]
\varepsilon^3 \mathscr{R}e\left(\partial_t v_r + v_x \partial_x v_r + \dfrac{1}{r} v_r \partial_r (r v_r)\right) = -\partial_r p_b + 2\dfrac{\varepsilon^2}{r} \partial_r\left(r\, \widetilde{G}(\dot\gamma)\, \partial_r v_r\right) + \varepsilon^2 \partial_x\left(\widetilde{G}(\dot\gamma)\, (\partial_r v_x + \varepsilon^2 \partial_x v_r)\right), \\[2mm]
\partial_x v_x + \dfrac{1}{r} \partial_r (r v_r) = 0,
\end{cases}
$$

where the dimensionless expression of the shear rate $\dot\gamma$ is given by

$$
\dot\gamma = \sqrt{|\partial_x v_x|^2 + |\partial_r v_r|^2 + \left|\dfrac{v_r}{r}\right|^2 + \dfrac{1}{2}\left|\dfrac{1}{\varepsilon}\partial_r v_x + \varepsilon \partial_x v_r\right|^2}.
$$

We note that the function $\widetilde{G}$ appearing in the above equations is related to G by $\widetilde{G}(\dot\gamma) = G\left(\dfrac{P\varepsilon^2}{\mu}\dot\gamma\right)$.

The dimensionless version of Darcy's low governing the flow in the membrane has the following form (see Section 3.1.2 for the dimensional form of these equations):

$$
\begin{cases}
\varepsilon^2 \partial_x^2 p_m + \dfrac{1}{r} \partial_r (r \partial_r p_m) = 0, \\[2mm]
u_x = -\dfrac{\mathscr{D}a}{\mathscr{P}_1} \partial_x p_m, \\[2mm]
u_r = -\dfrac{\mathscr{D}a}{\varepsilon^2\, \mathscr{P}_1} \partial_r p_m,
\end{cases}
$$

for every $(x, r) \in \omega_m$. Similarly to the blood flow, for every $(x, r) \in \omega_d$ and $t > 0$, the dimensionless dialysate flow is governed by the following system (see Section 3.1.3 for the dimensional form of these equations):

$$
\begin{cases}
\varepsilon \mathscr{R}e\,\mathscr{P}_1\left(\partial_t w_x + w_x \partial_x w_x + \dfrac{1}{r} w_r \partial_r (r w_x)\right) = -\partial_x p_d + \varepsilon^2 \mathscr{P}_1 \partial_x^2 w_x + \dfrac{\mathscr{P}_1}{r} \partial_r (r \partial_r w_x), \\[2mm]
\varepsilon^3 \mathscr{R}e\,\mathscr{P}_1\left(\partial_t w_r + w_x \partial_x w_r + \dfrac{1}{r} w_r \partial_r (r w_r)\right) = -\partial_r p_d + \dfrac{\varepsilon^2 \mathscr{P}_1}{r} \partial_r (r \partial_r w_r) + \varepsilon^4 \mathscr{P}_1 \partial_x^2 w_r, \\[2mm]
\partial_x w_x + \dfrac{1}{r} \partial_r (r w_r) = 0.
\end{cases}
$$

In order to complete the system, we add the dimensionless versions of the conditions on the interface blood/membrane (see Section 3.1.4 for the dimensional form of these equations):

$$\begin{cases} v_r = -\dfrac{\mathscr{D}a}{\varepsilon^2}\partial_r p_m, \\[2mm] -\partial_r v_x = B_b v_x, \qquad \text{for every } (x, r) \in \gamma_{bm}, \ t > 0, \\[2mm] p_m = p_b, \end{cases}$$

and on the interface membrane/dialysate, respectively (see Section 3.1.5 for the dimensional form of these equations):

$$\begin{cases} w_r = -\dfrac{\mathscr{D}a}{\varepsilon^2 \mathscr{P}_1}\partial_r p_m, \\[2mm] \partial_r w_x = B_d w_x, \qquad \text{for every } (x, r) \in \gamma_{md}, \ t > 0. \\[2mm] p_m = p_d - p_o, \end{cases}$$

Finally, we have the following boundary conditions, for every $t > 0$ (see Section 3.1.6 for the dimensional form of these equations):

$$\begin{cases} p_b|_{\gamma_{\ell,b}} = 1, \qquad\qquad\qquad p_b|_{\gamma_{r,b}} = 0, \\[2mm] p_d|_{\gamma_{r,d}} = -\mathscr{P}_2, \qquad\qquad p_d|_{\gamma_{\ell,d}} = -\mathscr{P}_2 - \mathscr{P}_1, \\[2mm] w_r|_{\gamma_d} = w_x|_{\gamma_d} = 0, \quad \partial_r v_x|_{\gamma_b} = 0 \end{cases}$$

where $\mathscr{P}_1$ and $\mathscr{P}_2$ are respectively given by (3.3) and (3.4).

Appendix B. Variational formulation

In order to numerically approximate the simplified system obtained in Section 3.3, we consider a weak formulation of the system. Since in Section 3.3 we obtained an explicit solution for the pressure p_m inside the membrane (domain ω_m), we write here the weak formulations only in the domains ω_b and ω_d.

• **Blood flow** (in ω_b):

$$\begin{cases} -\left[\displaystyle\int_0^{\frac{R_1}{R}} r p_b \varphi_1^b \,\mathrm{d}r\right]_{x=0}^{x=1} + \iint_{\omega_b} p_b r \partial_x \varphi_1^b \,\mathrm{d}x\,\mathrm{d}r - \int_{\gamma_{bm}} r \widetilde{G}(\dot{\gamma}) B_b v_x \varphi_1^b \,\mathrm{d}x \\[4mm] \qquad\qquad\qquad\qquad\qquad\qquad - \iint_{\omega_b} r \widetilde{G}(\dot{\gamma})\, \partial_r v_x \partial_r \varphi_1^b \,\mathrm{d}x\,\mathrm{d}r = \iint_{\omega_b} r \partial_x p_o \varphi_1^b \,\mathrm{d}x\,\mathrm{d}r, \\[4mm] \displaystyle\int_{\gamma_{bm}} p_b r \varphi_2^b \,\mathrm{d}x - \iint_{\omega_b} p_b (\varphi_2^b + r \partial_r \varphi_2^b) \,\mathrm{d}x\,\mathrm{d}r = 0, \\[4mm] \displaystyle\iint_{\omega_b} \partial_x v_x \varphi_3^b \,\mathrm{d}x\,\mathrm{d}r + \iint_{\omega_b} \frac{1}{r}\partial_r (r v_r)\varphi_3^b \,\mathrm{d}x\,\mathrm{d}r = 0, \end{cases}$$

for every $\varphi_i^b \in V_i^b$ and $i \in \{1, 2, 3\}$. These variational formulations are standard and V_i^b are Sobolev spaces endowed with the boundary conditions mentioned in Section 3.3. For more details on the variational formulations of equations used in modelling of fluid flows see, for instance, the monograph Glowinski (2003).

In order to take into account the boundary condition for v_r on γ_{bm}, it is convenient to make the following change of variable:

$$V_r = v_r + r\widetilde{K}_b(p_d - p_b + p_o), \text{ where } \widetilde{K}_b = \frac{\widetilde{\mathscr{D}}aR^2}{R_1^2 \ln(R_2/R_1)}.$$

Using this change of variable, the last equation describing the blood flow becomes

$$\iint_{\omega_b} \partial_x v_x \varphi_3^b \, dx \, dr + \iint_{\omega_b} \frac{1}{r}\partial_r(rV_r)\varphi_3^b \, dx \, dr - \iint_{\omega_b} 2\widetilde{K}_b(p_d - p_b + p_o)\varphi_3^b \, dx \, dr = 0,$$

for every $\varphi_3^b \in V_3^b$ and, therefore, V_r verifies $V_r = 0$ on γ_{bm}.

• **Dialysate flow** (in ω_d):

$$
\begin{cases}
-\left[\int_{\frac{R_2}{R}}^1 rp_d\varphi_1^d \, dr\right]_{x=0}^{x=1} + \iint_{\omega_d} p_d r\partial_x\varphi_1^d \, dx \, dr - \int_{\gamma_{md}} \mathscr{P}_1 r\partial_r w_x \varphi_1^d \, dx - \iint_{\omega_d} \mathscr{P}_1 r\partial_r w_x \partial_r\varphi_1^d \, dx \, dr = 0, \\[2mm]
\left[\int_0^1 p_d r\varphi_2^d \, dx\right]_{r=\frac{R_2}{R}}^{r=1} - \iint_{\omega_d} p_d(\varphi_2^d + r\partial_r\varphi_2^d) \, dx \, dr = 0, \\[2mm]
\iint_{\omega_d} \partial_x w_x \varphi_3^d \, dx \, dr + \iint_{\omega_d} \partial_r \frac{1}{r}(rw_r)\varphi_3^d \, dx \, dr = 0,
\end{cases}
$$

for every $\varphi_i^d \in V_i^d$, where V_i^d are standard Sobolev spaces endowed with the corresponding boundary conditions.

As in the case of the blood flow, in order to take into account the boundary condition for w_r on γ_{md}, the following change of variable is made:

$$W_r = w_r + (1 - r)\widetilde{K}_d(p_d - p_b + p_o), \text{ where } \widetilde{K}_d = \frac{\widetilde{\mathscr{D}}aR^2}{\mathscr{P}_1 R_2(R - R_2)\ln(R_2/R_1)}.$$

Therefore, the last equation describing the dialysate flow reads as:

$$\iint_{\omega_d} \partial_x w_x \varphi_3^d \, dx \, dr + \iint_{\omega_d} \frac{1}{r}\partial_r(rW_r)\varphi_3^d \, dx \, dr - \iint_{\omega_d} \frac{1-2r}{r}\widetilde{K}_d(p_d - p_b + p_o)\varphi_3^d \, dx \, dr = 0,$$

for every $\varphi_3^d \in V_3^d$. Hence, the new variable W_r satisfies $W_r = 0$ on γ_{md}.

In the remaining part of this appendix, we give the variational formulation corresponding to the rescaled system (4.4) modelling the evolution in time of the concentrations c_i.

• **Biochemical concentrations** (in ω):

The system (4.4) has the following variational formulation: find $c_i \in \mathscr{C}_i$ such that

$$\iint_\omega \partial_t c_i r \varphi_i \, dx \, dr + \iint_\omega S_i \left(U_x \partial_x c_i + U_r \partial_r c_i \right) r \varphi_i \, dx \, dr + \frac{1}{\mathscr{P}e} \iint_\omega r D_i \partial_r c_i \partial_r \varphi_i \, dx \, dr$$

$$- \frac{\varepsilon^2}{\mathscr{P}e} \int_{\gamma_{r,d}} r D_i \partial_x c_i \varphi_i \, dr$$

$$+ \frac{\varepsilon^2}{\mathscr{P}e} \int_{\gamma_{\ell,b}} r D_i \partial_x c_i \varphi_i \, dr + \frac{\varepsilon^2}{\mathscr{P}e} \iint_\omega r D_i \partial_x c_i \partial_x \varphi_i \, dx \, dr = \frac{1}{\mathscr{F}d} \iint_\omega r F_i(c_1, \ldots, c_5) \varphi_i \, dx \, dr,$$

for every $\varphi_i \in \mathscr{C}_i$, where $\mathscr{C}_i$ are Sobolev spaces taking into account the boundary conditions.

Appendix C. The gradient-type algorithm used for the minimization of the function $\mathscr{J}$.

In this appendix, we explicit an optimization algorithm employed to determine the pressure boundary data from the flow rate data. Given the flow rates $\vec{Q} \in \mathbb{R}^4$, we will minimize the function $\mathscr{J} : \mathbb{R}^4 \longmapsto \mathbb{R}^+$ defined by $\mathscr{J}(\vec{P}) = \frac{1}{2}\|\Phi(\vec{P}) - \vec{Q}\|^2$, the function Φ mapping a given pressure vector $\vec{P} \in \mathbb{R}^4$ onto the corresponding fluxes vector $\vec{Q} \in \mathbb{R}^4$ (this operation is carried out in Section 3.5.1 by directly solving the weak formulation which is well posed for given pressure data). The gradient-type algorithm that we use for the minimization of the function $\mathscr{J}$ is described in Algorithm 1.

GIVEN $\vec{P}, \varepsilon_1, h, \alpha_0$
$\alpha \leftarrow \alpha_0$
WHILE $\left(\alpha > \varepsilon_1 \right)$ DO
$\qquad \vec{S} \leftarrow \sum_{j=1}^{4} \frac{\mathscr{J}(\vec{P} + h\vec{e}_i) - \mathscr{J}(\vec{P})}{h} \vec{e}_i$
$\qquad$ DO
$\qquad\qquad \vec{P}^\star \leftarrow \vec{P} - \alpha \vec{S}$
$\qquad\qquad \alpha \leftarrow \alpha/10$
$\qquad$ UNTIL $\left(\mathscr{J}(\vec{P}^\star) \leq \mathscr{J}(\vec{P}) \text{ or } \alpha \leq \varepsilon_1 \right)$
$\qquad$ IF $\alpha > \varepsilon_1$ THEN
$\qquad\qquad \vec{P} \leftarrow \vec{P}^\star$
$\qquad\qquad \alpha \leftarrow \alpha_0$
END

Algorithm 1. A gradient-type algorithm used for the minimization of the function $\mathscr{J}$.